Journal of Geophysical Research: Atmospheres

RESEARCH ARTICLE
10.1029/2018JD029134

Special Section:
Studies of Emissions and Atmospheric Composition, Clouds and Climate Coupling by Regional Surveys, 2013 (SEAC4RS)

Biomass Burning Plumes in the Vicinity of the California Coast: Airborne Characterization of Physicochemical Properties, Heating Rates, and Spatiotemporal Features

Ali Hossein Mardi[1], Hossein Dadashazar[1], Alexander B. MacDonald[1], Rachel A. Braun[1], Ewan Crosbie[2,3], Peng Xian[4], Tyler J. Thorsen[3], Matthew M. Coggon[5], Marta A. Fenn[3], Richard A. Ferrare[3], Johnathan W. Hair[3], Roy K. Woods[6], Haflidi H. Jonsson[6], Richard C. Flagan[7], John H. Seinfeld[7], and Armin Sorooshian[1,8]

[1]Department of Chemical and Environmental Engineering, University of Arizona, Tucson, AZ, USA, [2]Science Systems and Applications, Inc., Hampton, VA, USA, [3]NASA Langley Research Center, Hampton, VA, USA, [4]United States Naval Research Laboratory, Monterey, CA, USA, [5]Cooperative Institute for Research in Environmental Science and National Oceanic and Atmospheric Administration, Boulder, CO, USA, [6]Naval Postgraduate School, Monterey, CA, USA, [7]Department of Chemical Engineering, California Institute of Technology, Pasadena, CA, USA, [8]Department of Hydrology and Atmospheric Sciences, University of Arizona, Tucson, AZ, USA

Abstract This study characterizes in situ airborne properties associated with biomass burning (BB) plumes in the vicinity of the California coast. Out of 231 total aircraft soundings in July–August 2013 and 2016, 81 were impacted by BB layers. A number of vertical characteristics of BB layers are summarized in this work (altitude, location relative to cloud top height, thickness, number of vertically adjacent layers, interlayer distances) in addition to differences in vertical aerosol concentration profiles due to either surface type (e.g., land or ocean) or time of day. Significant BB layer stratification occurred, especially over ocean versus land, with the majority of layers in the free troposphere and within 100 m of the boundary layer top. Heating rate profiles demonstrated the combined effect of cloud and BB layers and their mutual interactions, with enhanced heating in BB layers with clouds present underneath. Aerosol size distribution data are summarized below and above the boundary layer, with a notable finding being enhanced concentrations of supermicrometer particles in BB conditions. A plume aging case study revealed the dominance of organics in the free troposphere, with secondary production of inorganic and organic species and coagulation as a function of distance from fire source up to 450 km. Rather than higher horizontal and vertical resolution, a new smoke injection height method was the source of improved agreement for the vertical distribution of BB aerosol in the Navy Aerosol Analysis and Prediction System model when compared to airborne data.

Key Points:
- Significant biomass burning (BB) layer stratification with majority of layers in the free troposphere within 100 m of the boundary layer top
- A new smoke injection height method improved agreement for the vertical distribution of BB aerosol in the NAAPS model versus in situ data
- Shortwave heating rate profiles demonstrate the combined effect of stratocumulus cloud and BB layers and their mutual interactions

Supporting Information:
- Supporting Information S1
- Data Set S1

Correspondence to:
A. Sorooshian,
armin@email.arizona.edu

Citation:
Mardi, A. H., Dadashazar, H., MacDonald, A. B., Braun, R. A., Crosbie, E., Xian, P., et al. (2018). Biomass burning plumes in the vicinity of the California coast: Airborne characterization of physicochemical properties, heating rates, and spatiotemporal features. *Journal of Geophysical Research: Atmospheres*, *123*, 13,560–13,582. https://doi.org/10.1029/2018JD029134

Received 7 JUN 2018
Accepted 26 OCT 2018
Accepted article online 31 OCT 2018
Published online 5 DEC 2018

Author Contributions:
Conceptualization: Armin Sorooshian
Formal analysis: Ali Hossein Mardi
Funding acquisition: Armin Sorooshian
Investigation: Ali Hossein Mardi, Hossein Dadashazar, Alexander B. MacDonald, Rachel A. Braun, Ewan Crosbie, Peng Xian, Tyler J. Thorsen, Matthew M. Coggon, Marta A. Fenn, Richard A. Ferrare, Johnathan W. Hair, *(continued)*

1. Introduction

Biomass burning (BB) emissions are of growing concern in areas experiencing drier and warmer climates, such as the western United States, which has experienced larger and more frequent fires in recent decades (Dennison et al., 2014; Flannigan et al., 2000; Moritz et al., 2012). Particulate emissions resulting from fires affect radiative forcing, the hydrological cycle, air quality, and public health. To quantify these various BB aerosol effects, it is necessary to have knowledge about the vertical, spatial, temporal, and physicochemical nature of BB plumes. Owing to the expense and logistical complexity of conducting airborne measurements in BB plumes, there have been limited reports of such details with high resolution (e.g., Antokhin et al., 2018; Reid et al., 2005).

A region that is especially vulnerable to wildfires is the California coast, where several studies have examined aerosol and gas characteristics during cases of BB emissions (Akagi et al., 2012; de Gouw et al., 2003; Duong et al., 2011; Hawkins & Russell, 2010; Muhle et al., 2007; Sahu et al., 2012; Singh et al., 2010; Wonaschutz et al., 2011), with at least one report of BB interactions with boundary layer clouds (Brioude et al., 2009). Brioude et al. (2009) suggested that BB plumes reside well above the marine boundary layer within 500 km of the coastline, whereas farther away, BB aerosol entrains into the boundary layer. However, airborne in situ data were lacking in that work. Owing to the scarcity of detailed airborne measurements in BB plumes, there is a knowledge gap with regard to BB plume characteristics by the California coast, and generally other

Roy K. Woods, Haflidi H. Jonsson, Richard C. Flagan, John H. Seinfeld, Armin Sorooshian

Methodology: Ali Hossein Mardi, Armin Sorooshian

regions. Establishing the temporal and spatial scales of variability for BB plumes and their vertical proximity to clouds can help guide the resolution required by models and remote sensors attempting to resolve BB plumes and their effects.

Improving such knowledge can benefit models and remote sensors, which struggle with capturing BB plumes that require high spatial and temporal resolution. For example, models attempting to resolve BB aerosol layers as a function of altitude often rely on intercomparisons with remote sensing data, for example, the Cloud-Aerosol Lidar and Infrared Pathfinder Satellite Observation (CALIPSO) sensor (Walter et al., 2016). CALIPSO data pose challenges including reduced confidence in aerosol type classification in the proximity of thick cloud layers and presence of thick smoke near sources (Liu et al., 2009; Walter et al., 2016), as well as the base altitude of aerosol layers being biased too high leading to an underestimate in layer thickness and aerosol optical depth (AOD; Rajapakshe et al., 2017). Because of errors in both the Multiangle Imaging Spectroradiometer heights and Goddard Earth Observing System boundary layer heights, Martin et al. (2010) could only consider a smoke plume as being in the free troposphere (FT) with high confidence if it resided at least 500 m above the boundary layer top.

Studies of smoke-cloud interactions relying on columnar aerosol proxy measurements such as AOD are prone to retrieval artifacts near clouds and often address colocation issues by using passive fields from tracer transport models (e.g., for an insoluble species such as CO) with cloud fields viewed from satellites (Avey et al., 2007; Brioude et al., 2009). Vertically resolved airborne measurements of aerosols and clouds circumvent the aforementioned issues and can be used to better constrain the vertical and spatial extent of BB layers and their position relative to clouds (Kaufman et al., 2005; Painemal et al., 2014). The latter is important because the type and extent of impact of a BB plume on a cloud layer depend on the vertical distance between the two (Brioude et al., 2009; Johnson et al., 2004; Koch & Del Genio, 2010; Painemal et al., 2014; Yamaguchi et al., 2015). Furthermore, vertical profiles of BB plumes enable us to establish the extent to which the smoke plume is completely mixed in a column or consists of multiple single layers. A BB vertical profile near the source of the fire contains information on the smoke injection height and smoke column structure during injection (Kahn et al., 2008; Paugam et al., 2016; Sofiev et al., 2013). However, vertical aircraft sampling of BB plumes near wildfires is rare.

Aside from the dimensions and vertical details of BB plumes, the physicochemical properties of BB particles are also of major significance as they influence the extent to which particles interact with solar radiation and how effective they will be as cloud condensation nuclei (CCN) and ice nuclei. BB aerosols can undergo rapid evolution upon transport (Reid et al., 1998) and there exist uncertainties related to the nature of the composition and size distribution of particles in BB plumes (Pósfai et al., 2003). Moreover, essentially unknown is the relative abundance of coarse BB aerosol in the marine boundary layer, since such particles have important effects on clouds in the study region off the California coast (Dadashazar et al., 2017; Jung et al., 2015).

The goal of this work is to contribute to the limited inventory of airborne data of BB plume properties by analyzing data sets from two summer campaigns conducted along the California coast, which had extensive BB influence. This analysis focuses on examining (i) vertical profiles of aerosol concentration with and without BB influence as a function of time of day and location relative to the coastline to characterize spatiotemporal scales of BB layer variability; (ii) BB layering characteristics, that is, the number and location of observed BB layers in a vertical sounding including relative to clouds; (iii) the combined effect of cloud and BB layers and their mutual interactions with regard to vertical profiles of shortwave heating rates (SHRs); (iv) the extent of agreement between BB plume vertical distributions between airborne measurements and an aerosol transport model, including sensitivity tests with a new smoke injection method; and (v) size distribution and composition of BB particles.

2. Experimental Methods

2.1. Twin Otter Field Campaigns

Airborne data were analyzed from two separate campaigns based out of Marina, California, using the Center for Interdisciplinary Remotely-Piloted Aircraft Studies Twin Otter. The Nucleation in California Experiment (NiCE) took place in July–August 2013 and the Fog And Stratocumulus Evolution (FASE)

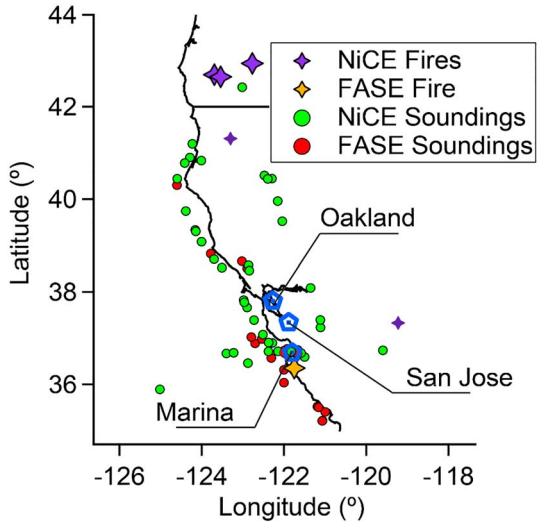

Figure 1. Spatial distribution of 81 aircraft soundings during NiCE (39 in green) and FASE (42 in red) that were influenced by biomass burning plumes. The smaller purple markers correspond to fires that were also present during the NiCE campaign; the one in northern California began after the original three to the north of the California-Oregon border, while the one to the east of Marina was too far to impact the airborne data.
NiCE = Nucleation in California Experiment; FASE = Fog And Stratocumulus Evolution.

experiment was conducted from July–August 2016. All relevant details about the aircraft measurements, including quality control and assurance protocols of each instrument, are summarized by Sorooshian et al. (2018). This work examined sounding data collected during NiCE and FASE. Locations of these soundings relative to the fire sources in NiCE and FASE are shown in Figure 1. Measurements at the end of the NiCE campaign were impacted by a series of forest fires near the California-Oregon border (Big Windy, Whiskey Complex, Douglas Complex; Sorooshian et al., 2015), in which smoke was advected parallel to the coast in a northerly/northwesterly direction (Maudlin et al., 2015). The majority of the FASE campaign was impacted by the Soberanes Fire in the vicinity of the Garrapta State Park, approximately 30 km southwest of Marina, California (Schlosser et al., 2017).

2.1.1. Aerosol and Gas Measurements

Aerosol size distributions were measured with a Passive Cavity Aerosol Spectrometer Probe (PCASP; Particle Measuring Systems, Inc., modified by Droplet Measurement Technologies, Inc.). The particle diameter (D_p) range varied between NiCE (0.12–2.95 μm) and FASE (0.12–3.42 μm). Submicrometer aerosol composition measurements were conducted during NiCE (unavailable in FASE) using a Compact Time-of-Flight Aerosol Mass Spectrometer (AMS; Aerodyne Research Inc.; Coggon et al., 2012) and a Particle-Into-Liquid Sampler (PILS; Brechtel Manufacturing Inc.) coupled to offline ion chromatography (Sorooshian et al., 2006). The AMS provided mass concentrations of nonrefractory species (organics, sulfate, nitrate, and ammonium), while the PILS-IC provided concentrations of water-soluble inorganic and organic acid species. Carbon monoxide measurements were conducted with a Los Gatos Research (LGR, Inc.) CO/CO_2 Analyzer during the FASE campaign. The PCASP and CO measurements were conducted at 1 Hz, whereas the AMS and PILS data were collected at ~10 s and ~5 min resolutions, respectively.

2.1.2. Meteorology and Cloud Measurements

Determination of cloud base and top heights was necessary in order to identify distances between BB layers and clouds. A PVM-100A probe (Gerber et al., 1994) and a Forward Scattering Spectrometer Probe (D_p ~2–45 μm; Particle Measuring Systems, Inc., modified by DMT, Inc.) were used to quantify liquid water content (LWC). While the PVM-100A probe provided LWC data during FASE, the Forward Scattering Spectrometer Probe was instead used during NiCE to quantify LWC owing to improved data quality. A threshold LWC value of 0.02 g/m^3 was applied to identify the presence of clouds as in previous work (Z. Wang et al., 2014, 2016). The temperature inversion base height was used to designate the top of the boundary layer. Temperature data were obtained with a Rosemount Model 102 total temperature sensor. All meteorological and cloud measurements were collected at 1 Hz time resolution.

2.2. NASA Airborne Lidar Data

To complement the Twin Otter data, simultaneous airborne data were used from NASA aircraft campaigns that coincided with NiCE and FASE. During NiCE in 2013, the NASA DC-8 conducted lidar measurements with the High Spectral Resolution Lidar (HSRL) technique (Hair et al., 2008) with the DIAL/HSRL instrument as part of the Studies of Emissions and Atmospheric Composition, Clouds and Climate Coupling by Regional Surveys campaign. The HSRL retrievals of vertical profiles of aerosol backscattering at 532 nm were used here, which had a nominal resolution of 30 m in the vertical and 2 km horizontally. The vertical coverage began at 30 m above ground level. During FASE in 2016, the NASA ER2 conducted HSRL-2 measurements as part of test flights for the ObseRvations of Aerosols above CLouds and their intEractionS (ORACLES). Similar to Studies of Emissions and Atmospheric Composition, Clouds and Climate Coupling by Regional Surveys, vertical profiles of aerosol backscattering at 532 nm were used, with vertical and horizontal resolutions of 30 m and 1.5 km, respectively. The overall systematic error associated with the 532 nm backscatter calibration is estimated to be <2–3%.

Table 1
RF, Date, and Number of Biomass Burning-Affected Soundings in Each RF for NiCE and FASE

Campaign	RF	Date	Only above	Above and below	Only below
NiCE	16	7/29/2013	4	1	—
	17	7/30/2013	4	—	2
	18	7/31/2013	1	—	—
	19	8/01/2013	2	—	—
	20	8/02/2013	7	1	2
	21	8/05/2013	2	—	—
	22	8/06/2013	2	1	—
	23	8/07/2013	10	—	—
FASE	3	7/25/2016	5	—	—
	4	7/26/2016	3	—	1
	5	7/27/2016	4	—	—
	6	7/29/2016	2	—	—
	7	8/01/2016	2	—	—
	8	8/02/2016	1	1	—
	9	8/03/2016	—	1	—
	10	8/04/2016	5	3	2
	11	8/05/2016	1	—	—
	13	8/09/2016	—	—	2
	14	8/10/2016	—	1	1
	15	8/11/2016	6	1	—

Note. Soundings are categorized based on where the biomass burning influence occurred: Only above = only above either cloud top (cloudy soundings) or inversion base height (clear soundings); Only below = only below cloud base; Above and below = both locations. Dates are formatted as month/day/year. RF = Research flight; NiCE = Nucleation in California Experiment; FASE = Fog And Stratocumulus Evolution. Dashes mean that there were no data available.

2.3. Aerosol Modeling

Predictions from the Navy Aerosol Analysis and Prediction System (NAAPS; Lynch et al., 2016; http://www.nrlmry.navy.mil/aerosol_web/) were contrasted with airborne in situ measurements. The default NAAPS version employed here relied on global meteorological fields from the Global Atmospheric Prediction System, now Navy Global Environmental Model (Hogan et al., 2014), and provided dust, sea salt, biomass-burning smoke, and anthropogenic and biogenic fine-mode aerosol data at a spatial resolution of 1° × 1°, at 6-hr intervals, and with 24 vertical levels below 100 mb. NAAPS data from a sensitivity simulation with finer spatial (1/3° × 1/3°) and vertical resolution (35 vertical levels below 100 mb) were also used. Smoke from BB was derived from near-real time satellite-based thermal anomaly data used to construct smoke source functions (Reid et al., 2009). Quality-controlled retrievals of AOD from the Moderate Resolution Imaging Spectroradiometer (Hyer et al., 2011; Zhang & Reid, 2006) were assimilated into the system. Model predictions were obtained from the grid pixel containing a particular Twin Otter sounding and linearly interpolated between the adjacent 6-hourly data points available based on the time of a sounding.

2.4. BB Layers

2.4.1. Criteria for BB Layer Bases and Tops

As one objective of this work was to characterize thicknesses of BB layers and distances between BB layers and other features, it was necessary to define height criteria for BB layer bases and tops. Owing to the scarcity of studies of this nature, there is no standard quantitative method for the detection of bases and tops of BB layers. Thus, here we present a method conducive to reproducibility of results (rather than subjective criteria) that could be used in future studies with commonly used aerosol instrumentation.

The quantitative tracer that was available in both campaigns and was consistently enhanced during times corroborated with the other BB observations (e.g., olfactory and visual evidence, CO) was PCASP aerosol number concentration (N_a). Past work in this study region (Prabhakar et al., 2014) and others (Capes et al., 2008; Johnson et al., 2008) have demonstrated the validity of PCASP data for BB detection. The specific criterion of N_a exceeding 1,000 cm^{-3} was calculated based on data from 352 vertical soundings collected over 73 research flights with no BB influence (based on visual/olfactory evidence and lack of particle concentration enhancement), as part of NiCE, FASE, and four other campaigns in the same study region (Sorooshian et al., 2018): the Marine Stratus/Stratocumulus Experiments (MASE I, MASE II), the Eastern Pacific Emitted Aerosol Cloud Experiment (E-PEACE), and the Biological and Oceanic Atmospheric Study (BOAS). For these 352 soundings, the average and standard deviation of N_a were calculated for the vertical layer of 0–200 m above cloud tops: 272 ± 223 cm^{-3}. The average plus three times the standard deviation was 941 cm^{-3}, which was rounded up to a stricter value of 1,000 cm^{-3}, to denote the minimum concentration needed to be established as BB aerosol. Contiguous vertical regions meeting this BB aerosol criterion qualified as a BB layer, and frequently, multiple BB layers were identified in a single aircraft sounding. Quantitative characteristics of BB layers discussed subsequently are sensitive to the BB layer base/top height criterion.

Out of a combined 231 Twin Otter soundings during NiCE and FASE, 81 were impacted by BB layers (39 in NiCE, 42 in FASE). Table 1 summarizes the flight number and dates of these 81 soundings. The highest density of soundings occurred near Marina (Figure 1), owing to ascents and descents associated with landing and taking off at the airport.

2.4.2. Distance From Fire Source

The distance from the fire sources to the sounding locations was calculated as a horizontal distance. With three separate sources of fires during NiCE within a relatively tight spatial area, the distance of each sounding from the fire source was calculated as the shortest distance between individual soundings and the closest

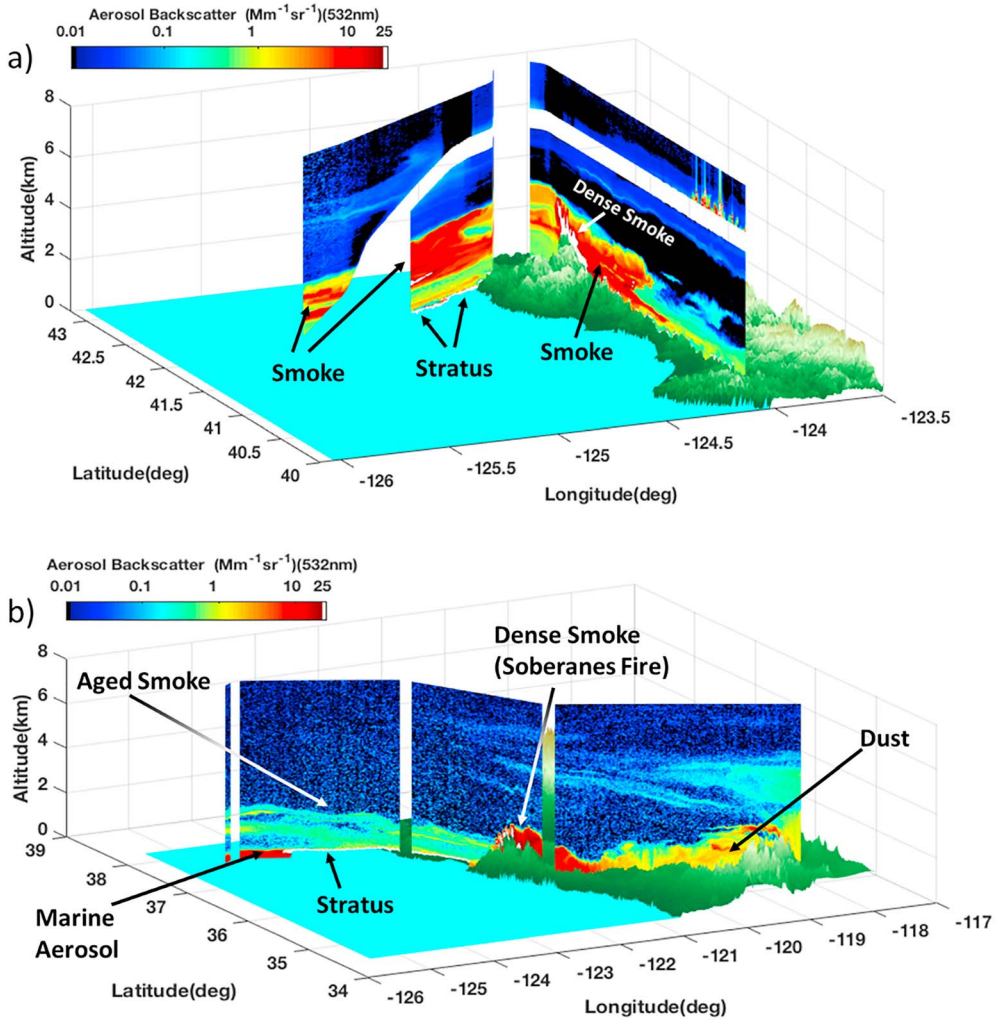

Figure 2. Vertically resolved aerosol backscatter data from (a) 6 August 2013 as measured by the DIAL/HSRL instrument on the NASA DC-8, and (b) 3 August 2016 from the HSRL-2 instrument on the NASA ER2 aircraft. These two flights coincide with the same fires examined in all other figures by the CIRPAS Twin Otter.

fire. Two other fires in California were identified during NiCE. One fire in northern California began on 1 August 2013 based on Moderate Resolution Imaging Spectroradiometer imagery, and overlapped with five of seven NiCE research flights for which BB-influenced data were collected. GOES imagery showed that the BB plumes from this fire moved mainly to the north in the direction of the original cluster of three fires. Based on its trajectory and close proximity to the other three fire spots to the north, it was considered to be grouped with the others, and the closest distance between a sounding and any of those three fires is still used for distance calculations. Another fire was identified much farther to the east of the sampling area, which was ruled out as influencing the flight data based on its distance and smoke trajectory patterns, as confirmed by GOES imagery.

3. Results and Discussion

3.1. Lidar Profiles of the 2013 and 2016 Fires

A spatial survey of the vertical tropospheric structure is provided in Figure 2 during both the 2013 and 2016 fire events using the NASA airborne lidar instruments. The aerosol backscatter data reveal that dense smoke was expectedly in the lower troposphere over the fire sources in both years of analysis, and that BB plumes were advected over the ocean within close vertical proximity to the stratus deck. The BB air masses detected

by the lidars had varying thicknesses and vertical layering behavior in the two case flights shown. For instance, during the 2013 flight, the BB plumes appeared to be lower in altitude farther away from the coastline, which was not the case in the 2016 flight with transported plumes at the same altitude (if not higher) than those near the coastline. Figure S1 shows more details related to trajectory analysis confirming that BB plumes were surveyed, the NASA aircraft flight tracks during the times of the lidar retrievals, and a time series view of the aerosol backscatter data. Differences observed during these two case flights motivate discussion of the more detailed Twin Otter measurements where multiple flights were conducted to quantify BB layer characteristics below, inside, and above the boundary layer.

3.2. Vertical Position of BB Layers

The injection height (height at which a buoyant plume begins to transport horizontally) and vertical position of BB plumes influence the lifetime and effects of BB particles in the atmosphere (e.g., Martin et al., 2010). BB aerosol injected into the FT will be transported farther as compared to BB aerosol residing in the boundary layer (Damoah et al., 2004; Labonne et al., 2007; Trentmann et al., 2002). Varying reports exist as to whether BB plumes reside mostly in the boundary layer versus the FT. In their analysis over North America with Multiangle Imaging Spectroradiometer data, Martin et al. (2010) showed that 4–12% of fire plumes were injected above the boundary layer. Labonne et al. (2007) showed with CALIPSO and European Centre for Medium-range Weather Forecast data that most BB plumes globally are initially limited to the boundary layer. Conditions of strong subsidence can result in trapping of BB emissions in the boundary layer, as was shown in southern Africa (Blake et al., 1996). Other work in that same region showed that only 20% of particles below 3 km were directly affected by BB in contrast to at least 67% of particles above 3 km due to convective lift from the heat of the fires (Pósfai et al., 2003). Similar observations of smoke layers residing above the boundary layer due to convective lifting have been noted over southern Africa and in the outflow over the southeast Atlantic Ocean (e.g., Chand et al., 2009; Keil & Haywood, 2003), in Asian continental outflow (Blake et al., 2003; Singh et al., 2003), off the California coast (Prabhakar et al., 2014), and over the Midwestern United States (Shingler et al., 2016). McMillan et al. (2008) tracked plumes originating over the Alaskan/Canadian Yukon region and traveling as far as Europe; the BB layer vertical position ranged from 3 to 11 km over Wisconsin based on surface lidar retrievals.

In contrast with the aforementioned results, the average base altitude of the lowest BB layer for all soundings was 782 ± 306 m (NiCE) and 537 ± 319 m (FASE; Table 1). Seventy-one of 81 total soundings (35 of 39 in NiCE and 36 of 42 in FASE) exhibited at least one BB layer in the FT, defined as being above either cloud top or the inversion base for cloud-free soundings. Some of those 71 soundings exhibited evidence of BB layers very close to cloud top, with 26 (9 in NiCE and 17 in FASE) exhibiting plume bases within 50 m above cloud top. Five and 15 soundings from NiCE and FASE, respectively, had BB layers extending from the FT into cloud top, indicative of entrainment. Ten total soundings exhibited evidence of BB layers only below cloud base, all in close proximity to the shoreline, suggestive of horizontal advection from the fire source to the marine boundary layer.

The presence of the overwhelming majority of BB layers in the FT instead of the boundary layer differs with results of Labonne et al. (2007) that suggested most BB plumes globally are initially limited to the boundary layer rather than higher in the FT. In contrast to the present work, that study suggested that the few cases of BB aerosol above the boundary layer over the western United States were not linked to active fires but instead atmospheric transport. The nature of the fire events we examined may have differed with regard to the heat and buoyancy near the fire source that helped propel the plumes into the FT. The ubiquity of BB aerosol in the FT during active fires in the present study region is important since the BB aerosol can both reside longer in the atmosphere owing to less efficient wet scavenging, and be transported farther (Labonne et al., 2007). Another possible explanations for why our results differ from those of Labonne et al. (2007) may include differences in data types used, where this study relied on airborne in situ data while the other used a combination of remote sensing and reanalysis data.

The proximity of BB layers to stratocumulus cloud tops has been suggested to have a greater effect on cloud properties than column aerosol loadings (Painemal et al., 2014). The distance separating cloud tops and the base of BB layers impacts the thermodynamic structure of the atmosphere, cloud properties, and radiative forcing (Haywood et al., 2003). This is especially important off the California coast, as past work suggested that BB plumes can be in close proximity to, and even entrained into, clouds (Brioude et al., 2009). Recent

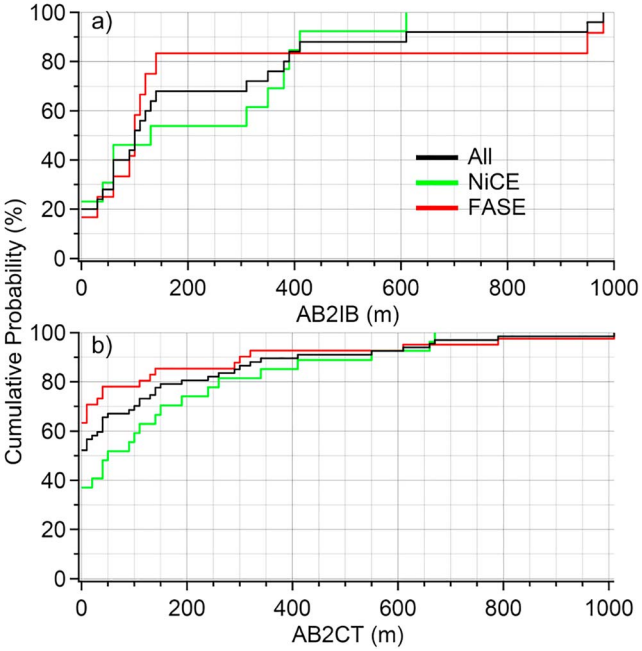

Figure 3. Cumulative probability of occurrence for distances between (a) aerosol base to inversion base (AB2IB; for cloud-free soundings) and (b) aerosol base to cloud top (AB2CT; for cloudy soundings). Aerosol bases refer to the base altitude of biomass burning layers. NiCE = Nucleation in California Experiment; FASE = Fog And Stratocumulus Evolution.

work for the southeastern Atlantic Ocean with NASA's Cloud-Aerosol Transport System lidar showed that the aerosol layer base is lower than previously thought based on CALIPSO data (Costantino & Breon, 2010; Keil & Haywood, 2003; Labonne et al., 2007; Painemal et al., 2014; Yu et al., 2012), and within 360 m of cloud tops (Rajapakshe et al., 2017). Devasthale and Thomas (2011) showed in a global CALISPO survey that the distance between clouds and aerosol layers exceeded 100 m in 90–95% of cases examined between June 2006 and May 2010. For reference, past work has considered a physical separation of less than 100 m as a situation in which aerosols and clouds interact, whereas a minimum threshold distance of 750 m was classified as a *well-separated* scene (Costantino & Breon, 2013); the same authors previously considered 250 m as a dividing threshold between smoke and clouds being well separated or interacting (Costantino & Breon, 2010).

Figure 3 reports a summary of the distance between the base of the first BB layer observed above cloud tops relative to cloud top height (termed *AB2CT* by Rajapakshe et al., 2017, to represent aerosol layer bottom to cloud top height). In cloud-free soundings, *AB2IB* is calculated to represent distance from the BB aerosol base to inversion base. As multiple BB layers were observed in some soundings, only the lowest one was considered in this analysis. A key result of Figure 3 is that majority of soundings exhibited a BB layer within 100 m of the boundary layer top, regardless of field campaign. BB layers entrained into cloud top in 20 soundings, while there were six such instances of entrainment of BB aerosol from the FT into the boundary layer in cloud-free soundings. Excluding cases of BB aerosol entrainment into the boundary layer, the average (± standard deviation) AB2CT and AB2IB distances in FASE were 235 ± 299 m (n = 16) and 263 ± 350 m (n = 10), respectively, while in NiCE they were 235 ± 208 m (n = 17) and 269 ± 181 m (n = 10). The presence of clouds did not seem to play a large role in affecting the distance of BB layers relative to the top of the boundary layer, and two different summer's worth of fires yielded similar BB layer separation from cloud tops (cloudy soundings) and inversion base heights (cloud-free soundings). For the FASE cases examined, AB2CT distances reached as high as 1,006 m, with AB2IB distances peaking at 979 m. For NiCE, the AB2CT and AB2IB distances reached as high as 664 and 606 m, respectively. The variabilities in AB2CT and AB2IB were governed more by BB layer base altitude as compared to cloud top altitude and inversion layer base altitude, respectively, based on linear regression analysis (Figure S2): AB2CT versus cloud top altitude: $r = -0.17$, AB2CT versus BB layer base altitude: $r = 0.75$; AB2IB versus inversion layer base altitude: $r = 0.41$, AB2IB versus BB layer base altitude: $r = 0.91$.

As the results in Figure 3 did not reveal significant differences between NiCE and FASE, the data were combined to next examine the cumulative probability of occurrence of AB2CT and AB2IB over land versus ocean (Figure S3). The average AB2CT over the ocean was 165 ± 272 m (n = 41), in contrast to 74 ± 141 m over land (n = 10). The average AB2IB over land was higher (410 ± 345 m; n = 11) than over the ocean (170 ± 166 m; n = 19). As there was similarity between cloud top heights over land (538 ± 189 m) and ocean (509 ± 201 m) and inversion base heights over land (334 ± 88 m) and ocean (302 ± 210 m), variations in BB layer altitudes (Ocean: cloudy = 674 ± 312 m, clear = 502 ± 371 m; Land: cloudy = 613 ± 208 m, clear = 844 ± 373 m) were more responsible for the significant differences in AB2CT and AB2IB over land versus ocean.

3.3. Vertical Thickness of BB Layers

The vertical thickness of BB layers is relevant for characterizing BB emission effects on clouds and the thermodynamic structure of the atmosphere, in addition to providing guidance on the vertical resolution of models and remote sensing retrievals aiming to accurately represent BB plume structure. Intercomparing results between studies is challenging, however, owing to the difficulty of defining bases and tops of plumes in a consistent way between in situ and remote sensing techniques. In their global survey of BB layers using CALIPSO data, Devasthale and Thomas (2011) reported that 70–80% of their cases exhibited layers less

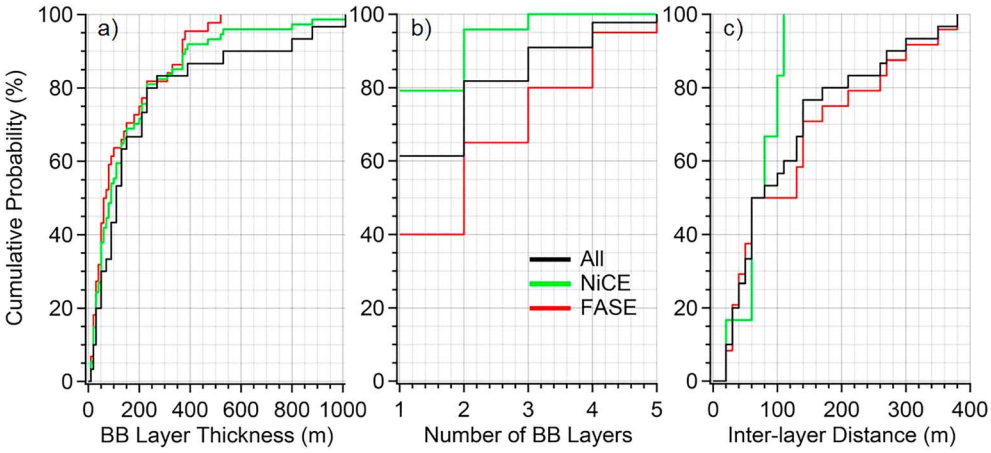

Figure 4. Cumulative probability of occurrence for (a) BB layers of varying thicknesses, (b) number of BB layers observed during BB-influenced soundings, and (c) distance between BB layers. For a fair comparison between soundings, the data in all panels correspond to soundings up to a fixed 700 m above either the cloud top height (cloudy soundings) or inversion base height (cloud-free soundings). NiCE = Nucleation in California Experiment; FASE = Fog And Stratocumulus Evolution; BB = biomass burning.

than 1 km thick, while 18–22% of cases were 1–2 km thick. During NiCE and FASE, a significant fraction of layers were $<$100 m thick (13 of 30 in NiCE and 28 of 44 in FASE; Figure 4a). The average thicknesses were 204 ± 257 m (NiCE) and 128 ± 137 m (FASE). The thickest layer observed was 1,010 m from NiCE RF20 on 2 August 2013. The thinnest layer was 6 m observed in RF4 of FASE (26 July 2016).

The extent to which single or multiple BB layers exist in an atmospheric column matters with regard to the vertical thermodynamic profile and points to the level of vertical mixing versus stratification. The rise of aerosol plumes above the boundary layer in the FT is thought to be governed by atmospheric stability, specifically the presence of stratified layers (Kahn et al., 2007). Martin et al. (2010) showed in their study over North America that 86% of BB plumes had stable layers associated with them. Figure 4b summarizes the cumulative probability of occurrence for varying numbers of BB layers for both cloudy and cloud-free soundings. For a fair comparison, soundings were compared only when the aircraft measured up to the same altitude above either cloud top height (cloudy soundings) or inversion base height (cloud-free soundings), chosen to be 700 m to reflect a balance between having substantial separation from the boundary layer top and a reasonable sample size. The most common number of BB layers observed was one (Figure 4b). Seven out of 35 and 12 out of 36 soundings in NiCE and FASE, respectively, were characterized as having multiple BB layers. The highest number of layers in any single sounding in NiCE and FASE was three and seven, respectively, but only four out of seven layers of the latter sounding from FASE campaign were considered in Figure 4b as the base of fifth layer is located above 700 m from cloud top (i.e., 990 m). For soundings with multiple BB layers, the minimum-maximum distances between layers for NiCE and FASE were 18–104 and 13–372 m, respectively (Figure 4c). During NiCE, the majority of cases (5 of 6) exhibited a gap less than 100 m between vertically adjacent BB layers. During FASE, 12 of 24 cases exhibited a gap less than 100 m between layers.

Non-BB impacted soundings were further analyzed to determine whether stratification in the FT is an inherent characteristic of the region or if it is only observed in conjunction with an abundance of absorbing BB particles in the FT. There was evidence of stratification of aerosol layers in non-BB impacted soundings. A representative example shown from NiCE RF11 on 22 July 2013 (Figure S4) displays several distinct layers of enhanced N_a (each exceeding 600 cm^{-3}) above the cloud layer in the FT, coincident with enhancements in specific humidity. Therefore, the stratification of aerosol layers observed in the study region is not limited just to BB aerosol, but also other transported aerosol plumes such as continental biogenic plumes (Coggon et al., 2014).

3.4. Vertical Aerosol Concentration Profiles

Figure 5 compares N_a vertical profiles between cloudy soundings in the presence and absence of BB influence. FASE exhibited higher concentrations as compared to NiCE owing to closer proximity of

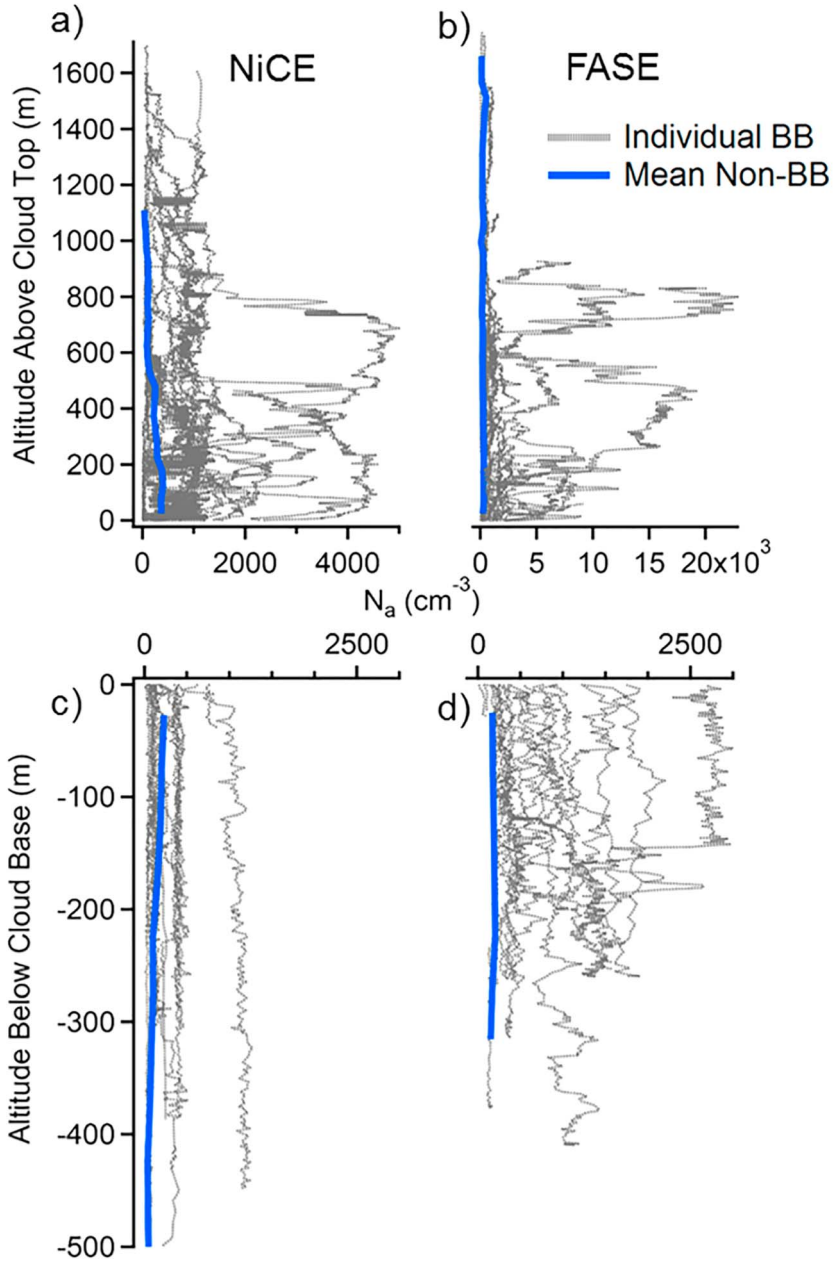

Figure 5. Vertical profiles of Passive Cavity Aerosol Spectrometer Probe aerosol concentration (N_a) from soundings impacted by BB on cloudy days over the ocean for (a, c) NiCE and (b, d) FASE. Individual BB profiles are in gray and the average of *background* (i.e., no BB influence) profiles are shown in thicker blue for contrast. (a–b) Vertical profiles beginning at cloud top, with cloud top representing an altitude of 0 m. (c–d) Vertical profiles in the subcloud region, with cloud base representing an altitude of 0 m. NiCE = Nucleation in California Experiment; FASE = Fog And Stratocumulus Evolution; BB = biomass burning.

measurements to the fire source. Much higher N_a values were observed in the FT versus the boundary layer in both campaigns. The mean N_a profiles below cloud base exhibited much higher concentrations in the BB soundings as compared to non-BB soundings for FASE, as most of those soundings were closer to the fire source as compared to NiCE.

Concentrations of N_a in the boundary layer tended to be more vertically homogeneous as compared to the FT, owing to more mixing and turbulence, as demonstrated previously for the study region based on aerosol size distribution data (Dadashazar et al., 2018). More specifically, for the nine soundings exhibiting evidence

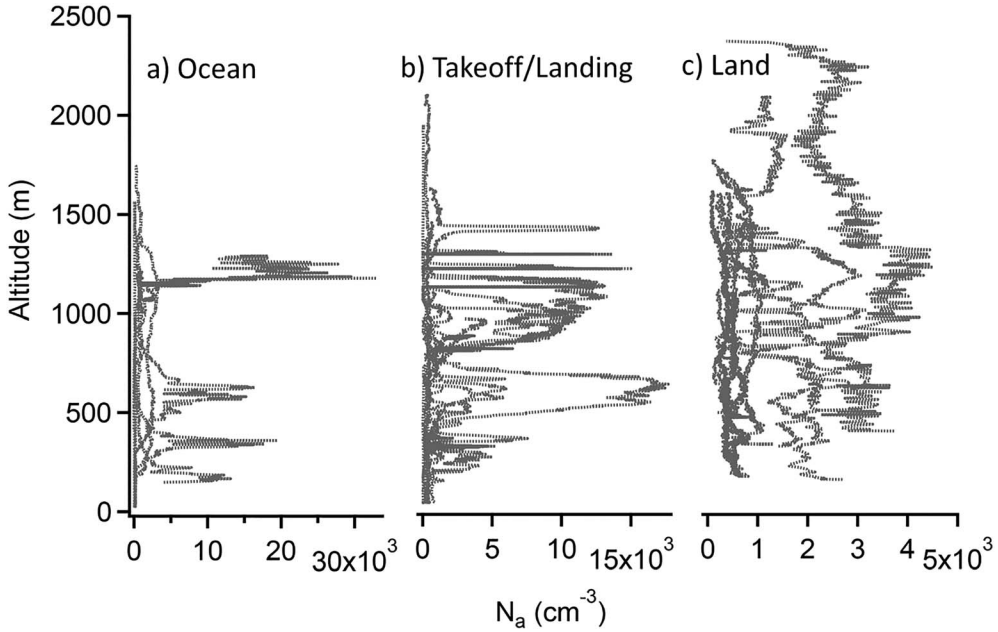

Figure 6. Comparison of Passive Cavity Aerosol Spectrometer Probe N_a vertical profiles over the (a) ocean, (b) airport take-offs and landings, and over (c) land (excluding take-offs and landings) during biomass burning-impacted soundings in Nucleation in California Experiment and the and Fog And Stratocumulus Evolution experiment. (Locations of all soundings are in Figure S4.) Data are only shown for cloud-free soundings to avoid issues with Passive Cavity Aerosol Spectrometer Probe data in cloud during cloudy soundings.

of BB layers both below and above cloud, the standard deviation of the N_a values for the profiles below and above cloud were 165 and 839 cm^{-3}, respectively. Among these nine cases, there were three cloud-free soundings, and thus data were compared below and above the inversion base for those cases. The corresponding ratios of standard deviation to mean were 0.14 (below cloud base or inversion base) and 0.56 (above cloud top or inversion base), which supports there being more mixing in the boundary layer as compared to the FT.

Owing to differences in thermodynamic profiles over land and water, it was expected that vertical aerosol profiles would vary also between different surface types during the fire events. NiCE and FASE offered an opportunity to compare the vertical aerosol structure during soundings conducted over land, ocean, and in the intermediate coastal area within ~30 km of the coastline where takeoffs and landings occurred by Marina (referred to as *Takeoff/Landing*; see Figure S5 for close-up of sounding locations). Figure 6 shows vertical profiles of N_a for individual soundings and as grand averages for all three locational categories. N_a values are more vertically homogeneous for the land category in contrast to the ocean and Takeoffs/Landing categories. When comparing N_a between 200 and 1,700 m, representative of common altitudes sampled in the majority of individual soundings shown, the average (± standard deviation) values were as follows: land = 792 ± 742 cm^{-3}; ocean = 1307 ± 1723 cm^{-3}; Takeoff/Landing = 1428 ± 2118 cm^{-3}. The reduced standard deviation, especially relative to the mean, in the land category is indicative of more mixing and less stratification of BB layers.

To put Figure 6 in context, aircraft measurements during the Southern African Regional Science Initiative (SAFARI 2000), based in Namibia, showed that BB aerosol was well mixed from the surface to approximately 5 km over land due to convection promoted by strong surface heating (Haywood et al., 2003). In contrast, over the ocean, BB aerosol was enriched between 3 and 5 km with elevated levels still down to 1.5 km; however, below 1.5 km there was distinctly cleaner air where the stratocumulus cloud layer resided. Statistics from 31 vertical profiles in that study revealed a mean BB layer altitude of 4.9 km (±0.7 km). The base of the layers could only be observed over the ocean (1.5 ± 0.6 km) in contrast to over land where vertical mixing extended the layer to the surface. Our data are generally consistent with the results of Haywood et al. (2003) in that more distinct layering existed over the ocean, with most layers in the FT. The soundings over land were

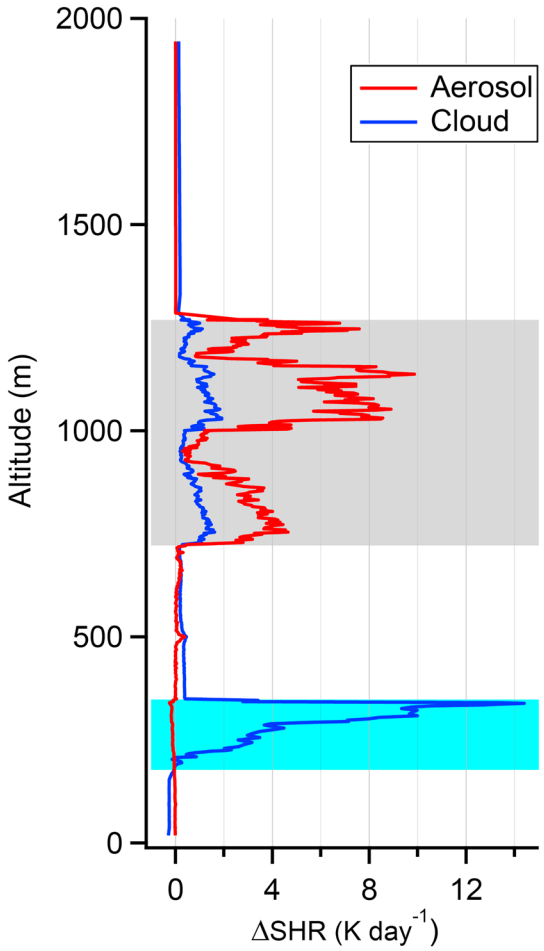

Figure 7. Vertical profiles of the impact of the aerosol and cloud on the SHR using data from a sounding starting at 19:20:40 UTC during Fog And Stratocumulus Evolution RF3 (25 July 2016). Specifically shown are the differences between the total SHR and either having no aerosol (ΔSHR in red) or no cloud (ΔSHR in blue). The light blue shading represents the cloud layer and the gray shaded region represents BB aerosol ($N_a > 1{,}000$ cm^{-3}). SHR = shortwave heating rate.

in conditions of stronger surface heating, and thus mixing, which resulted in less N_a variability with altitude. While the aircraft could not reach the surface for all soundings, calculations for potential temperature (θ) were conducted at the lowest common altitude possible (175 m) for the three categories, which confirmed that the land category was warmest: 291.6 ± 5.9 K (land), 287.1 ± 0.8 K (Takeoff/Landing), 286.0 ± 1.2 K (ocean).

3.5. Heating Rates

BB layers can absorb solar radiation and generate localized heating. For example, when comparing two adjacent soundings in FASE RF3 (25 July 2016) sampled within 50 km and 30 min of each other, there was a 4.2 K enhancement in θ for the BB impacted sounding relative to that not impacted by BB. Mesoscale buoyancy perturbations are generally rapidly damped out through gravity wave adjustment processes (Bretherton & Smolarkiewicz, 1989) and although part of the anomaly may be dynamically associated with the orography and complex flow patterns along the California coast, it is nonetheless interesting that such a substantial temperature anomaly be collocated with the smoke plume. It was of interest to quantify the SHR associated with BB plumes and how that heating could be impacted by the presence of a cloud underneath. Data from the BB-impacted sounding starting at 19:20:40 UTC during FASE RF3 were used to estimate diurnally averaged heating rates of the cloud layer, BB layer, and the interactions between them. A Mie theory calculation (Bohren & Huffman, 1983) was used to estimate the aerosol scattering cross section and phase function for each PCASP size bin. The real refractive index is assumed to be 1.53 at all wavelengths consistent with airborne observations (at 532 nm) in BB plumes (Aldhaif et al., 2018; Shingler et al., 2016). The results were then combined with the observed aerosol size distributions to produce estimated profiles of total scattering and asymmetry factor across the 0.175–4.0 μm wavelength range. Extinction and absorption were then estimated using a spectrally independent single scattering albedo of 0.95, consistent with airborne observations in BB plumes (Corr et al., 2012).

The aerosol scattering properties were used to compute the broadband shortwave radiative heating using the NASA Langley Fu-Liou radiative transfer model (Fu & Liou, 1992; Rose et al., 2013). The effects of liquid cloud droplets were included using the measured LWC and effective radius following Hu and Stamnes (1993). The standard midlatitude summer profile (McClatchey et al., 1972) was used to fill in above and below the airborne-based profiles. The broadband surface albedo was set to an ocean-like value of 0.05. The diurnally averaged radiative heating rates were obtained by averaging calculations over 10 solar zenith angles that evenly sample the distribution of angles that occurred on 25 July 2016.

Figure 7 isolates the impact of the aerosol and cloud on the SHR profile by taking the difference between the total SHR and the SHR computed without the aerosol or cloud in the profile. The differences were computed from the individual SHR profiles shown in Figure S6. The magnitude of the heating in the BB layer (layer mean) is approximately 4 K/day, large enough that it may be a significant component in the column heat budget with possible implications for layer static stability and the vertical diffusion of the smoke. The heating rate at cloud top is slightly reduced (−0.25 K/day) by the reduction in downwelling shortwave radiation caused by the BB layer, suggesting that shortwave radiative effects that influence the diurnal breakup or thinning of stratocumulus are not strongly modulated by a BB layer of this magnitude. Nevertheless, the dynamics of stratocumulus clouds have been shown to be quite sensitive to shortwave absorption (Caldwell et al., 2005; Turton & Nicholls, 1987). The heating rate in the BB layer is enhanced by the presence of the cloud (+0.8 K/day), because of an increase in upwelling shortwave radiation as a result of the high cloud albedo. This implies that marine boundary layer clouds can have an important influence on the

stratification and evolution of overlying smoke, with implications for how smoke layers subsequently descend and interact with, and entrain into, cloud.

3.6. Temporal Variability

The temporal scale of variability of BB plumes vertically and horizontally is important with regard to development of models and satellite products that aim to capture the location and effects of BB air masses. To address this, numerous cases of pairs of soundings were conducted during a flight in the same area but separated in time by several hours. These pairs of soundings were compared to examine the extent of variability in BB characteristics with time. The criteria employed here to compare soundings in the same area consisted of them being within a radial distance of 10 km. Figure 8 shows results for four case flights where soundings were conducted with ~4–10 hr of separation in nearly the same location. In all cases, the sounding later in the day exhibited higher θ values. For each case, the temperature inversion occurred at cloud top height for the first sounding, while the second sounding occurred in cloud-free air.

The 31 July 2013 case (Figure 8a) was characterized by a distinct BB plume above cloud top in the earlier sounding (~15:00 UTC), which was entirely absent 4 hr later (~19:00 UTC). The same trend was observed in the 29–30 July 2016 case (Figure 8b), which was the lone case over land and where the soundings were ~10 hr apart. In contrast, the 2 August 2016 case (Figure 8c) had a BB layer sampled at nearly the same altitude (480 m) separated in time by 5 hr (~18:00 and ~23:00 UTC); the earlier sounding exhibited BB influence below cloud and in another higher layer in the FT, both of which were not present 5 hr later. Lastly, the 11–12 August 2016 case (Figure 8d) was characterized by having the same BB layer in the FT around 600 m, but the earlier case had strong BB influence below cloud that was absent 8 hr later. The disappearance of BB layers in each case examined likely can be explained by transport and, in the case of the boundary layer, potentially wet scavenging. The results have implications for the use of one-time data snapshots in a particular day, whether it be from satellites, aircraft, or surface-based monitoring stations. Figure 8 demonstrates that the vertical profile of BB characteristics can change dramatically in as short as 4 hr, which was the shortest gap in time that was studied here.

NAAPS predictions of the vertical profile of smoke mass concentration are shown in Figure 8 corresponding to the same times of our soundings in the grid cell containing the location of the soundings. Different from the sounding profiles where lofted smoke layers are often observed, NAAPS smoke vertical profiles exhibit a bottom-heavy shape, with the maximum smoke concentration close to the surface for all four cases. The cause of the bottom-heavy shape and results of sensitivity tests to determine ways of improving NAAPS representation of the vertical profile of BB aerosol is provided in section 3.9. Figure 8b is a noteworthy comparison that shows that smoke was present in the early day sounding but disappeared later in the day, while NAAPS shows heavy smoke at both times. Satellite true-color images from Terra (10:30 A.M. local pass time) and Aqua (1:30 P.M. local pass time) for that day (https://worldview.earthdata.nasa.gov/) showed that severe smoke was present both in the morning and afternoon within the 1° and 1/3° model boxes tested with NAAPS in this study within which the soundings were taken. The fact that the sounding later in the day almost did not detect any smoke is most probably due to atmospheric transport placing the smoke plume right off the sounding location.

3.7. Aerosol Size Distributions

Aerosol number size distributions were examined owing to the importance of particle size for interactions with solar radiation and being able to act as CCN. It has been reported that BB aerosols are dominated by accumulation mode particles (hence, the usefulness of the PCASP probe) with their count mean radius generally increasing with aging owing to coagulation and condensation (e.g., Capes et al., 2008; Johnson et al., 2008; Reid et al., 2005). Figure 9 compares the average aerosol size distributions below and above clouds with and without BB influence for both campaigns, while Table S1 summarizes the count median diameter (CMD) and geometric standard deviation (σ_g) for the eight categories. NiCE size distributions clearly exhibit reduced particle concentrations as compared to FASE, in addition to having broader distributions extending from the lowest size cutoff of the PCASP (~0.11 μm) to supermicrometer sizes ($D_p > 1$ μm). The CMD (σ_g) values above and below cloud were 0.34 μm (1.89) and 0.39 μm (1.79) in BB conditions, respectively; the corresponding values in non-BB conditions were 0.21 μm (1.59) and 0.30 μm (1.84). In contrast, FASE distributions exhibited a narrower submicrometer number concentration peak, with higher

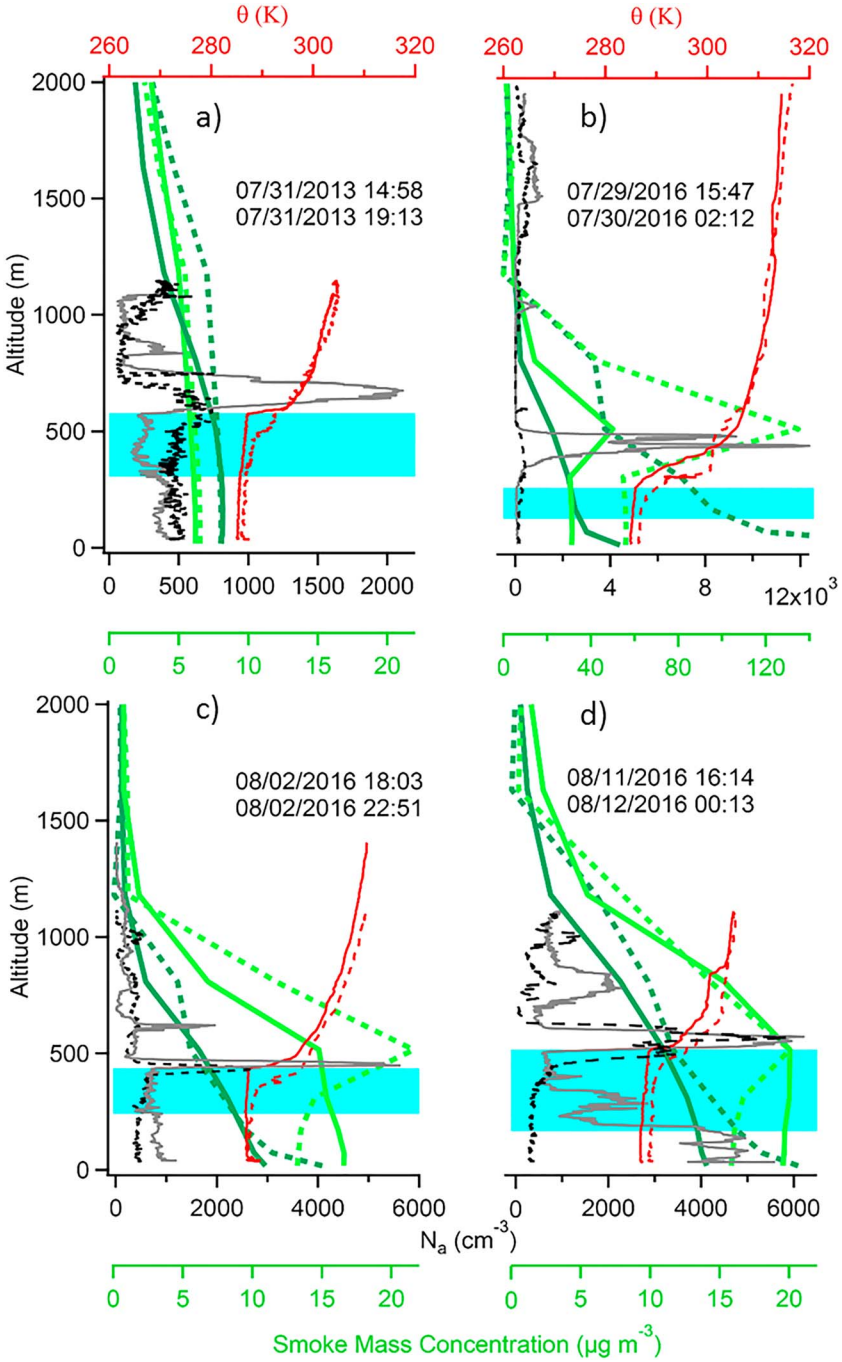

Figure 8. Vertical profiles of Passive Cavity Aerosol Spectrometer Probe N_a, potential temperature (θ), and Navy Aerosol Analysis and Prediction System smoke mass concentrations for pairs of aircraft soundings within 10 km of one another at different UTC times shown in each panel for (a) Nucleation in California Experiment RF18, (b) FASE RF6, (c) FASE RF8, and (d) FASE RF15. The average position of each sounding pair, using the 500 m altitude point of each sounding, was as follows: (a) 36.67°N, −121.64°W, (b) 36.64°N, −121.65°W (over land), (c) 36.71°N, −121.79°W, (d) 36.70°N, −121.82°W. Reported times in each panel are the point in each sounding when the aircraft was at 500 m altitude. Dashed lines represent data for the sounding later in the day. Horizontal blue rectangles represent cloud depth for the first sounding; the second soundings were in cloud-free air. For Navy Aerosol Analysis and Prediction System smoke mass concentration, the light green line corresponds to data obtained after applying a corrected smoke injection height at the source of fire and the dark green line corresponds to vertical profiles of smoke mass concentrations obtained for a regular injection height. FASE = Fog And Stratocumulus Evolution; RF = Research flight.

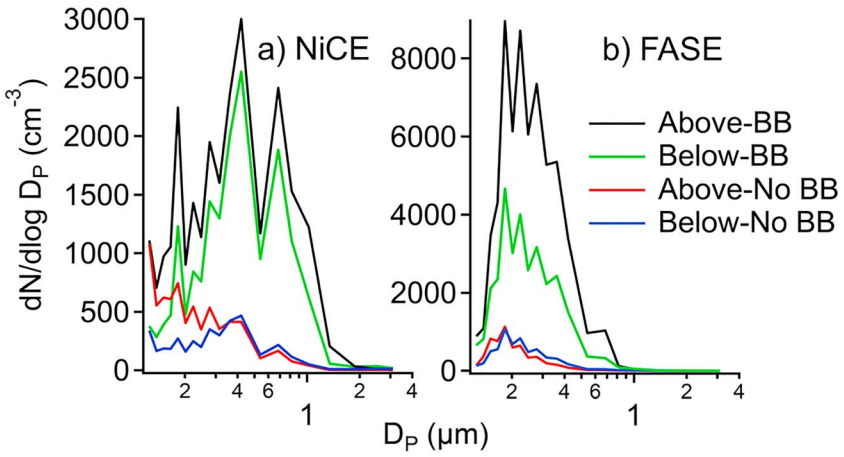

Figure 9. Average Passive Cavity Aerosol Spectrometer Probe aerosol size distributions during the (a) NiCE and (b) FASE campaigns for cloudy conditions. The average size distribution for BB-influenced areas are calculated only for periods when Passive Cavity Aerosol Spectrometer Probe N_a exceeded 1,000 cm^{-3}. The mean aerosol size distributions in non-BB conditions are calculated within 500 m above cloud top (for *Above*) and below the cloud base (for *Below*). The number of soundings used for obtaining the mean aerosol size distribution for non-BB and BB conditions above cloud was 7 and 21 for NiCE, respectively, and 58 and 19 for FASE. The corresponding number of soundings used to calculate mean size distributions below cloud for non-BB and BB conditions was 7 and 1 for NiCE, and 37 and 11 for FASE. NiCE = Nucleation in California Experiment; FASE = Fog And Stratocumulus Evolution; BB = biomass burning.

number concentrations below ~0.3 μm and a sharper decline in concentration above 1 μm. The CMD (σ_g) values above and below cloud were 0.24 μm (1.40) and 0.24 μm (1.46) in BB conditions, respectively; the corresponding values in non-BB conditions were 0.17 μm (1.36) and 0.19 μm (1.38). Differences between campaigns presumably exist due to a combination of different plume ages being sampled and different fuel types, as the NiCE fire cluster was characterized by *timber, grass and shrub models* (https://inciweb.nwcg.gov/incident/3562/) and the FASE fire included *chaparral, tall grass, and timber* (https://inciweb.nwcg.gov/incident/4888/; Braun et al., 2017).

Of particular interest in this study was the relative abundance of coarse aerosol in BB layers, as such particles represent giant CCN and can promote changes in cloud properties (Dadashazar et al., 2017; Jung et al., 2015). Jung et al. (2015) showed that salt particles (D_p: 1–10 μm) with concentrations up to 0.01 cm^{-3} were sufficient to result in a fourfold enhancement in cloud base rain rate. The percentage contribution of supermicrometer particles to total N_a above cloud during NiCE was 1.31 ± 1.99% (32.63 ± 74.62 cm^{-3}) and 0.25 ± 0.14% (0.88 ± 0.66 cm^{-3}) with and without BB influence, respectively. One case above cloud with BB influence reached as high as 8.90% (336.19 cm^{-3}). In contrast, the percentage contribution was 1.56% (17.08 cm^{-3}; no standard deviation due to one case) and 2.46 ± 1.54% (4.94 ± 3.59 cm^{-3}) below cloud with and without BB influence, respectively. The higher percentages below cloud versus above cloud can be attributed largely to sea salt. During FASE, the percentages above cloud with and without BB influence were 0.04 ± 0.02% (1.26 ± 0.96 cm^{-3}) and 0.10 ± 0.07% (0.22 ± 0.13 cm^{-3}), respectively, while the corresponding values below cloud were 0.17 ± 0.09% (2.69 ± 3.58 cm^{-3}) and 0.45 ± 0.33% (0.79 ± 0.40 cm^{-3}). The contributions of supermicrometer particles to total N_a were lower in FASE below and above cloud, as compared to NiCE, owing likely to some combination of sampling more concentrated plumes closer to the source, different plume ages and trajectories, and different fuel types. Although the reported percentages are small, the absolute concentrations of supermicrometer particles were enhanced in BB conditions and sufficiently high to impose important effects on clouds if entrainment were to occur (e.g., Jung et al., 2015). Surface-based aerosol measurements in Marina, CA, during NiCE showed strong evidence for dust as being the major source of those particles (Maudlin et al., 2015). More broadly, Schlosser et al. (2017) showed that dust is enhanced in concentration during wildfires as compared to non-fire periods across the western United States. The mixing of dust with BB aerosol was also observed over West Africa with airborne measurements (Johnson et al., 2008).

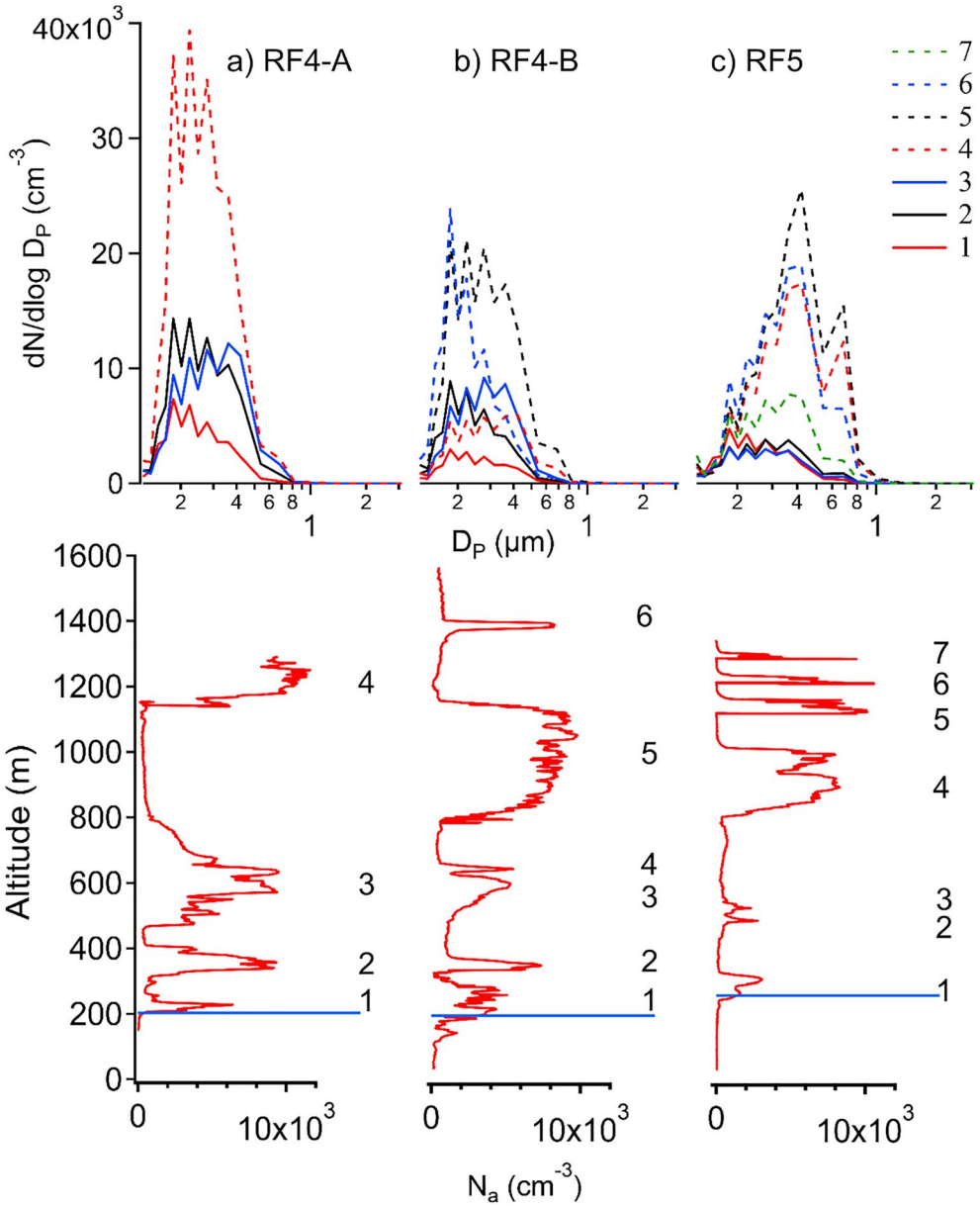

Figure 10. Three selected cases studies from Fog And Stratocumulus Evolution showing Passive Cavity Aerosol Spectrometer Probe aerosol size distributions for soundings with multiple biomass burning layers: (a) RF4-A: 26 July 2016, (b) RF4-B: 26 July 2016, (c) RF5: 27 July 2016. These three soundings correspond to either take-offs or landings. The top row of panels shows vertically averaged aerosol size distributions for each biomass burning layer, and the bottom row of panels shows the corresponding vertical distribution of total N_a for each case. Labels 1–7 represent the order of layers with ascending height (1 = lowest, 7 = highest), with the boundary layer top height marked with a blue line. RF = Research flight.

It was of interest to determine if differences in size distributions existed between vertically adjacent BB layers. This analysis was conducted for three soundings with a high number of layers (4–7; Figure 10). Two of the soundings were from FASE RF4 (26 July 2016) and one was from FASE RF5 (27 July 2016). These three case soundings show that on a case basis, there was considerable variability in the structure of the size distribution depending on the vertical position of the layer, suggestive of varying degrees of processing in different layers. The number concentration of supermicrometer particles generally tended to increase toward the lower layers, reaching as high as up to 7.37 cm^{-3} (see Table S2 for quantitative results).

3.8. Plume Aging Case Study

BB can be reflected in vertical profiles of aerosol species, especially organic aerosol (e.g., Alves et al., 2011; Formenti et al., 2003; Heald et al., 2011; Kondo et al., 2011; Reid et al., 1998; Sahu et al., 2012; Simoneit, 2002). As composition measurements were only available during NiCE, two research flights with nearly similar tracks (Figure S7) were compared to determine the extent to which submicrometer composition varied between BB and non-BB periods. The sections of the flights compared were along the coastline stretching from the source of the fire toward Marina, over which Maudlin et al. (2015) showed the predominant wind direction was mainly northwesterly in a manner somewhat parallel to the coastline. AMS composition data were compared when $N_a > 1{,}000\ cm^{-3}$ (for the BB influenced cases) and the aircraft altitude was above 700 m in the FT. PILS samples were included in the analysis that overlapped with the aforementioned criteria, but owing to the longer time resolution of the PILS (~5 min) and documented mixing effects in the instrument (Sorooshian et al., 2006), data also included periods with reduced BB influence ($N_a < 1{,}000\ cm^{-3}$) as compared to the AMS (~10 s).

Total mass concentrations during BB periods were significantly higher, with the AMS measurements exceeding the PILS owing to the abundance of nonrefractory organic species that the PILS-IC method cannot speciate (Figures 11a–11b). Interestingly though, the relative abundance of AMS species was rather similar during BB and non-BB periods, with organics accounting for 93% and 87% of the total mass concentration, respectively. Nitrate, sulfate, and ammonium each accounted for between 1% and 5% of the total mass. The PILS data (Figures 11c–11d) offer a view of the water-soluble chemical profile, with the BB mass profile dominated by ammonium (45%), followed by nitrate (17%), sulfate (11%), and calcium (9%). Ground-based measurements in Marina during NiCE showed that these species were also enhanced during the period of the wildfires, with the exception of calcium (Maudlin et al., 2015); however, the presence of dust in the BB plumes could be the source of the calcium, which may have been scavenged by clouds during transport of the plumes toward Marina. Of the various organic acid species measured, oxalate was the most abundant, accounting for 4% (0.20 $\mu g/m^3$) of the total PILS mass (4.74 $\mu g/m^3$). During non-BB periods, the PILS chemical profile was very different, with sulfate (43%), nitrate (22%), sodium (16%), and chloride (7%) accounting for most of the total mass concentration (0.72 $\mu g/m^3$). In contrast to BB periods, oxalate was negligible (~0%), while the sum of other organic acids measured (succinate, glutarate, adipate, maleate) were enhanced in their contribution (6%, 0.04 $\mu g/m^3$).

To examine the evolution of the BB plume composition downwind from the fire source in RF17, Figure 11e shows a time series of the AMS species concentration, while Table S3 summarizes how composition changed across different thirds of the flight leg extending from the fire source toward Marina (i.e., 0–~150, ~150–~300, ~300–~450 km). Although the mass concentrations changed significantly, the mass fractions stayed relatively similar for the entire flight duration. The only species exhibiting an increase in concentration with distance from the fire source was sulfate, which nearly tripled (0.12 to 0.34 $\mu g/m^3$) resulting in an enhancement of its mass fraction, albeit small (0.01 to 0.03). Except for sulfate, the minimum concentrations of all species occurred in the middle third of the flight, suggestive that the effects of dilution and any other loss processes such as volatilization had mostly taken place already and that there could have been production occurring downwind in the last two thirds of the flight. The mass concentrations of all species in even the last two thirds of the flight were higher than those in the non-BB flight.

Other work has shown that organics emitted directly from BB can be semivolatile but that their aging can reduce volatility and promote new organic aerosol formation via photochemistry (e.g., Grieshop et al., 2009). Extensive reports exist of secondary production of organics (e.g., Hawkins & Russell, 2010) and inorganics (e.g., sulfate, nitrate, ammonium) in BB plumes (Formenti et al., 2003; Gao et al., 2003; Reid et al., 1998; Yokelson et al., 2009), including for a chaparral fire by the central California coast in 2009 (Akagi et al., 2012). The latter study also pointed out an initial decrease in organic levels downwind of a fire source followed by a slow rise again (i.e., recondensation of species that evaporated initially), which coincides with the RF17 results. Our data provide support for secondary production of these same nonrefractory species in BB plumes up to a distance of ~450 km from the fire source, but without much change in their relative amounts. The latter has implications for hygroscopicity, which is more sensitive to the relative amounts of these species.

A time series summary of the PCASP aerosol number size distribution during this flight period revealed both higher overall concentrations closer to the fire source, especially for particles larger than 0.50 μm, and the

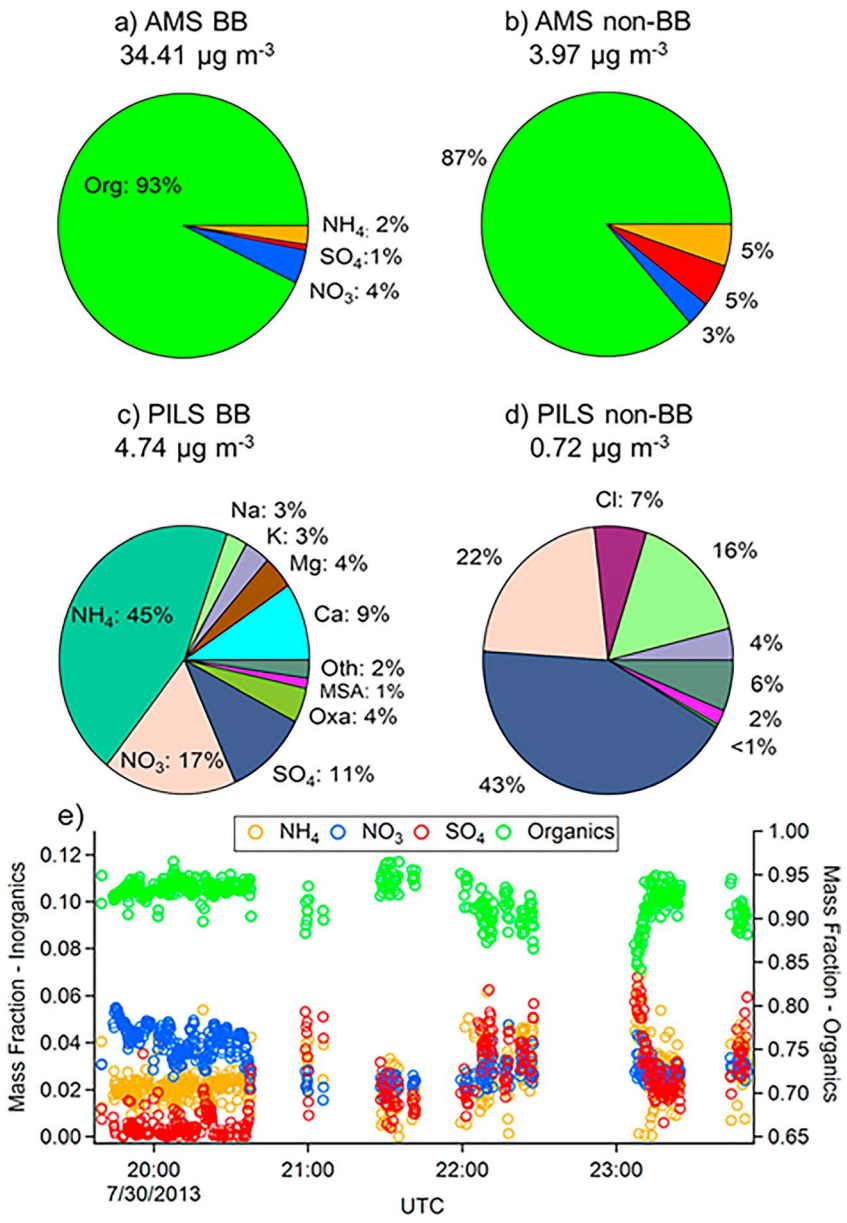

Figure 11. Pie chart comparison of submicrometer aerosol composition during free troposphere sampling in (a, c) BB conditions in Nucleation in California Experiment RF17 on 30–31 July 2013, and (b, d) non-BB conditions in Nucleation in California Experiment RF10 on 19–20 July 2013, and (e) variations in nonrefractory portion of aerosols as a function of time. This section of flight begins above the source of fire and due to semistraight flight track, time of flight is representative of the age of plume. Total mass concentrations are shown above each pie for the (a, b) AMS and (c, d) PILS measurements. The color labeling scheme in (a) and (c) are the same as those for (b) and (d) and the color labeling scheme in (e) is the same as (a) and (b). Oxa = oxalate; Oth = sum of succinate, glutarate, adipate, and maleate. AMS = Aerosol Mass Spectrometer; BB = biomass burning; PILS = Particle-Into-Liquid Sampler.

presence of multiple modal sizes (Figure S8). Expectedly, dilution resulted in reduced N_a as a function of plume age. There was also evidence of growth of smaller aerosol into larger size bins owing most likely to coagulation based on a negative relationship between the N_a value for two representative D_p ranges (0.12–0.16 vs 0.50–1.21 μm) when plumes with total Na exceeded 3,000 cm^{-3} during this flight; more specifically, the correlation between the natural logarithm of N_a between 0.12 and 0.16 μm versus N_a between 0.50 and 1.21 μm revealed a linear best fit line with $r = -0.95$ (Figure S9).

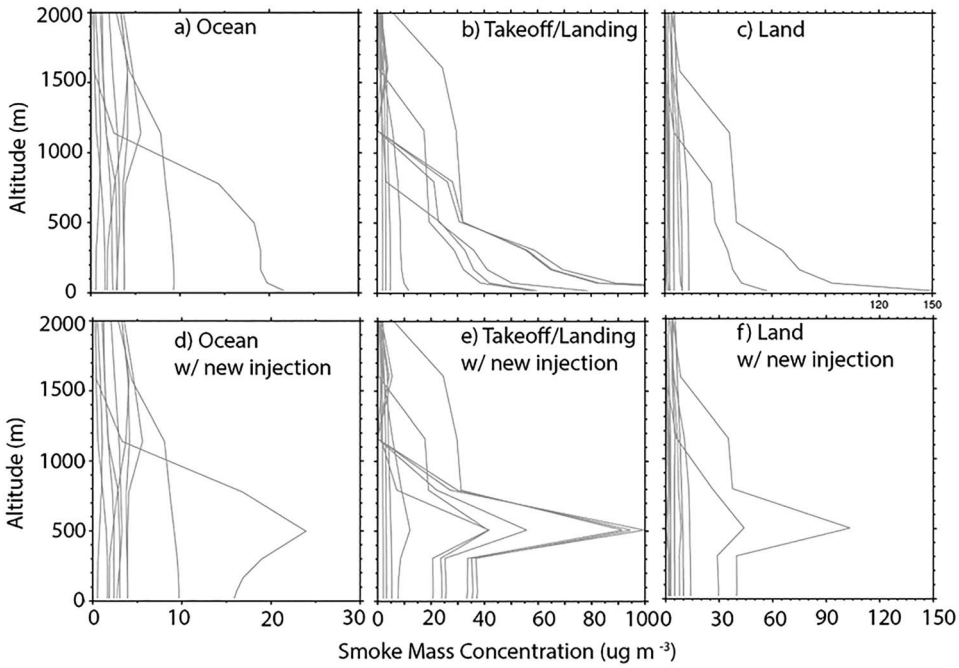

Figure 12. Navy Aerosol Analysis and Prediction System simulated smoke concentration vertical profiles paired (using the nearest neighbor interpolation in space and time) with the biomass burning-impacted soundings for over ocean, airport take-offs/landings, and over land, as shown in Figure 6. Profiles derived from Navy Aerosol Analysis and Prediction System with the default smoke injection method are shown in (a)–(c). Profiles derived with the new smoke injection method are shown in (d)–(f).

3.9. Evaluation of the Aerosol Transport Model

NAAPS was shown in many case studies to be able to capture long-range transport of BB smoke well. For example, it captured smoke aerosol amount transported over the Maritime Continent in field studies (Atwood et al., 2017; Reid et al., 2016) and over a range of time-scales (days, months, years) and different weather patterns over the Maritime Continent (Reid et al., 2012, 2015; Xian et al., 2013). NAAPS was also shown to have skill in capturing the timing and vertical distributions of smoke transported to the Arctic region from boreal wildfire events (Markowicz et al., 2017). Verified with space-borne and ground-based remote sensing column-total AOD products (2-dimensional), NAAPS performs well, in general, for large-scale BB smoke distribution (Lynch et al., 2016). However, there has been very limited work done to verify NAAPS vertical profiles using field study data. The NiCE and FASE field measurements provided such an opportunity to evaluate NAAPS aerosol vertical distribution during summer wildfire events over the central California coast.

As expected, NAAPS captures the smoke aerosol occurrence arising from the wildfire activities (see, e.g., movie in Data S1 made with 6-hourly smoke AOD distribution for the 2016 FASE campaign time). Recent work has revealed that NAAPS AOD may be biased low for the region affected by the Soberanes Fire during the study time based on evaluation of performances by a multimodel ensemble and individual models as compared with ground-based Aerosol Robotic Network AOD (P. Xian, personnel communication, 1 September 2018). In that study, all of the aerosol models exhibited high AOD root-mean-square error over the area impacted by the Soberanes Fire, suggesting the challenge all aerosol models face to accurately simulate the magnitude of smoke aerosol resulting from a major wildfire.

In this study, interest is placed on the verification of smoke vertical distributions of NAAPS. NAAPS smoke concentration profiles are paired with the soundings shown in Figure 6 and into the ocean, land, and take-off/landing categories (Figures 12a–12c). Quite different from the soundings, the model does not show distinct thin BB layers, but generally exhibits bottom-heavy shaped vertical profiles both over land and for the takeoff/landing category, with smoke mass concentration peaking near the surface. Over ocean, only a few

profiles show lofted BB layers, although very thick in depth because of the coarse vertical resolution. Multilayering structure is not resolved as was observed by the aircraft measurements.

As transport and vertical distributions of BB smoke are shown to be sensitive to smoke injection height in many aerosol modeling studies (Colarco et al., 2004; Ge et al., 2017; J. Wang et al., 2013), another NAAPS simulation, aiming for possible improvement of the vertical distribution of smoke for the NiCE and FASE cases, is tested using the observed average BB layer height as the smoke injection height (approximately 500 m based on the soundings). The default model smoke injection method is to inject smoke mass into the lowest four model layers, with the fourth layer centered around 300 m above ground. In the new set of simulations that were conducted, only the smoke injection method was different, and atmospheric processes within the model (e.g., mixing, transport, removal of the smoke aerosols) were treated the same way. With the new injection height, the modeled smoke vertical profiles are improved, and lofted smoke layers appear in many cases to more closely resemble sounding profiles, although not always (Figures 12d–12e and 8). For example, in the 29 July 2016, 02 August 2016, and 11 August 2016 cases in Figure 8, the new run yield lofted smoke layers centered around 500 m, close to the soundings. The smoke layers are generally thicker and more diffuse in the vertical compared to the sounding profiles, and there appear to be a few profiles with a second weak smoke layer around 1,600 m.

In another sensitivity test, NAAPS was run at higher horizontal and vertical resolutions (1/3° × 1/3° vs 1° × 1°, and 12 levels vs 6 levels below 1 km) compared to the default simulation. With the default smoke injection method, this high resolution simulation yielded similar bottom-heavy smoke vertical profiles. If a model does not have an initial injection mechanism (either through smoke injection parameterization or representation of fire meteorology, which is lacking in most meteorological models) to send smoke into the FT, and there exists a stable inversion layer above the smoke, the majority of smoke would most likely stay within the boundary layer. This could have resulted in the bottom-heavy profiles in the simulations with the default injection method, independent of model resolutions. This stresses the importance of smoke injection method/height for an aerosol model in capturing smoke vertical distributions over fire-prone regions such as the California coast and the need for developers of smoke emission inventories to include smoke injection height information in their data. The verification of NAAPS vertical profiles with the data collected during the NiCE and FASE campaigns provides a guide for model improvement.

4. Conclusions

This study reports on a characterization of BB plumes in the vicinity of the California coast using airborne measurements in two separate summertime campaigns (NiCE 2013, FASE 2016). Based on defined criteria using PCASP data, 81 soundings were impacted by BB layers. BB layers were detected both above and below the top of the boundary layer, but mainly in the FT with significant stratification, especially over the ocean as compared to land. While a single BB layer was most common, there were numerous cases of multiple BB layers. The vertical nature of BB aerosol was shown to change significantly within a period of just 4 hr in the same area. Bases of the lowermost BB layer in most soundings were within 100 m above the top of the boundary layer. The presence of clouds did not seem to play a large role in affecting the distance of BB layers relative to the top of the boundary layer, and two different summer's worth of fires yielded similar BB layer separation from cloud tops and inversion base heights. Intercomparison between the vertical profiles of BB aerosol between aircraft data and the NAAPS was shown to be significantly improved after changing the default smoke injection method to a revised method of injecting smoke at the observed average smoke layer height based on aircraft data (~500 m). This change was shown to be much more important as compared to improving horizontal and vertical resolution in the model. These sensitivity exercises and the successful intercomparison with the new smoke injection technique provides a guide for model improvement.

Heating rate calculations revealed several interesting features for a representative case study with a BB layer above cloud: (i) there was significant heating in the BB layer (4 K/day); (ii) the heating rate at cloud top was marginally reduced by the BB layer (~0.25 K/day); and (iii) the heating rate in the BB layer was enhanced due to the presence of the cloud (0.8 K/day). These results are significant owing to their implications for layer static stability (and thus vertical mixing of smoke), diurnal breakup and thinning of stratocumulus clouds when there is smoke, and tendencies of BB plumes to descend and interact with clouds.

Size distribution data were different between the two campaigns owing likely to different plume ages being sampled and different fuel types. Measurements in BB layers revealed higher values of CMD and σ_g as compared to non-BB air masses. High levels of supermicrometer particles occurred in BB conditions both above and below clouds, with implications for impacts on cloud properties. Considerable variability existed in size distributions between vertically adjacent BB layers, including an increase in the number concentration of supermicrometer particles in the layers closest to the top of the boundary layer.

The nonrefractory composition of submicrometer aerosol was dominated by organics in the FT, regardless of whether BB conditions existed or not; however, the mass concentration was significantly enhanced in BB conditions. Water-soluble composition, on the other hand, exhibited more differences between BB and non-BB conditions in the FT, with ammonium and oxalate being the most abundant inorganic and organic acid species, respectively. In non-BB conditions, sulfate was the most abundant species and oxalate was below detection limits. A case study was presented to show that over 450 km downwind of a fire source, the mass fractions of nonrefractory aerosol constituents exhibited very little change, while the data were suggestive of production of secondary organic and inorganic constituents, in addition to growth of particles via coagulation.

Acknowledgments

All data used in this work can be found on the Figshare database (Sorooshian et al., 2017; https://figshare.com/articles/A_Multi-Year_Data_Set_on_Aerosol-Cloud-Precipitation-Meteorology_Interactions_for_Marine_Stratocumulus_Clouds/5099983). This work was funded by Office of Naval Research grants N00014-10-1-0811, N00014-11-1-0783, N00014-10-1-0200, N00014-04-1-0118, and N00014-16-1-2567, and NASA grant NNX14AP75G.

References

Akagi, S. K., Craven, J. S., Taylor, J. W., McMeeking, G. R., Yokelson, R. J., Burling, I. R., et al. (2012). Evolution of trace gases and particles emitted by a chaparral fire in California. *Atmospheric Chemistry and Physics*, *12*(3), 1397–1421. https://doi.org/10.5194/acp-12-1397-2012

Aldhaif, A. M., Stahl, C., Braun, R. A., Moghaddam, M. A., Shingler, T., Crosbie, E., et al. (2018). Characterization of the real part of dry aerosol refractive index over North America from the surface to 12 km. *Journal of Geophysical Research: Atmospheres*, *123*, 8283–8300. https://doi.org/10.1029/2018JD028504

Alves, C., Vicente, A., Nunes, T., Goncalves, C., Fernandes, A. P., Mirante, F., et al. (2011). Summer 2009 wildfires in Portugal: Emission of trace gases and aerosol composition. *Atmospheric Environment*, *45*(3), 641–649. https://doi.org/10.1016/j.atmosenv.2010.10.031

Antokhin, P. N., Arshinova, V. G., Arshinov, M. Y., Belan, B. D., Belan, S. B., Davydov, D. K., et al. (2018). Distribution of trace gases and aerosols in the troposphere over Siberia during wildfires of summer 2012. *Journal of Geophysical Research: Atmospheres*, *123*(4), 2285–2297. https://doi.org/10.1002/2017JD026825

Atwood, S. A., Reid, J. S., Kreidenweis, S. M., Blake, D. R., Jonsson, H. H., Lagrosas, N. D., et al. (2017). Size-resolved aerosol and cloud condensation nuclei (CCN) properties in the remote marine South China Sea—Part 1: Observations and source classification. *Atmospheric Chemistry and Physics*, *17*(2), 1105–1123. https://doi.org/10.5194/acp-17-1105-2017

Avey, L., Garrett, T. J., & Stohl, A. (2007). Evaluation of the aerosol indirect effect using satellite, tracer transport model, and aircraft data from the international consortium for atmospheric research on transport and transformation. *Journal of Geophysical Research*, *112*, D10S33. https://doi.org/10.1029/2006JD007581

Blake, N. J., Blake, D. R., Simpson, I. J., Meinardi, S., Swanson, A. L., Lopez, J. P., et al. (2003). NMHCs and halocarbons in Asian continental outflow during the Transport and Chemical Evolution Over The Pacific (TRACE-P) field campaign: Comparison with PEM-West B. *Journal of Geophysical Research*, *108*(D20), 8806. https://doi.org/10.1029/2002JD003367

Blake, N. J., Blake, D. R., Sive, B. C., Chen, T. Y., Rowland, F. S., Collins, J. E., et al. (1996). Biomass burning emissions and vertical distribution of atmospheric methyl halides and other reduced carbon gases in the South Atlantic region. *Journal of Geophysical Research*, *101*(D19), 24151–24164. https://doi.org/10.1029/96JD00561

Bohren, C. F., & Huffman, D. R. (1983). *Absorption and scattering of light by small particles* (pp. 82–114). New York: John Wiley.

Braun, R. A., Dadashazar, H., MacDonald, A. B., Aldhaif, A. M., Maudlin, L. C., Crosbie, E., et al. (2017). Impact of wildfire emissions on chloride and bromide depletion in marine aerosol particles. *Environmental Science & Technology*, *51*(16), 9013–9021. https://doi.org/10.1021/acs.est.7b02039

Bretherton, C. S., & Smolarkiewicz, P. K. (1989). Gravity-waves, compensating subsidence and detrainment around cumulus clouds. *Journal of the Atmospheric Sciences*, *46*(6), 740–759. https://doi.org/10.1175/1520-0469

Brioude, J., Cooper, O. R., Feingold, G., Trainer, M., Freitas, S. R., Kowal, D., et al. (2009). Effect of biomass burning on marine stratocumulus clouds off the California coast. *Atmospheric Chemistry and Physics*, *9*(22), 8841–8856. https://doi.org/10.5194/acp-9-8841-2009

Caldwell, P., Bretherton, C. S., & Wood, R. (2005). Mixed-layer budget analysis of the diurnal cycle of entrainment in southeast pacific stratocumulus. *Journal of the Atmospheric Sciences*, *62*(10), 3775–3791. https://doi.org/10.1175/Jas3561.1

Capes, G., Johnson, B., McFiggans, G., Williams, P. I., Haywood, J., & Coe, H. (2008). Aging of biomass burning aerosols over West Africa: Aircraft measurements of chemical composition, microphysical properties, and emission ratios. *Journal of Geophysical Research*, *113*, D00C15. https://doi.org/10.1029/2008JD009845

Chand, D., Wood, R., Anderson, T. L., Satheesh, S. K., & Charlson, R. J. (2009). Satellite-derived direct radiative effect of aerosols dependent on cloud cover. *Nature Geoscience*, *2*(3), 181–184. https://doi.org/10.1038/Ngeo437

Coggon, M. M., Sorooshian, A., Wang, Z., Craven, J. S., Metcalf, A. R., Lin, J. J., et al. (2014). Observations of continental biogenic impacts on marine aerosol and clouds off the coast of California. *Journal of Geophysical Research: Atmospheres*, *119*, 6724–6748. https://doi.org/10.1002/2013JD021228

Coggon, M. M., Sorooshian, A., Wang, Z., Metcalf, A. R., Frossard, A. A., Lin, J. J., et al. (2012). Ship impacts on the marine atmosphere: Insights into the contribution of shipping emissions to the properties of marine aerosol and clouds. *Atmospheric Chemistry and Physics*, *12*(18), 8439–8458. https://doi.org/10.5194/acp-12-8439-2012

Colarco, P. R., Schoeberl, M. R., Doddridge, B. G., Marufu, L. T., Torres, O., & Welton, E. J. (2004). Transport of smoke from Canadian forest fires to the surface near Washington, D. C.: Injection height, entrainment, and optical properties. *Journal of Geophysical Research*, *109*, D06203. https://doi.org/10.1029/2003JD004248

Corr, C. A., Hall, S. R., Ullmann, K., Anderson, B. E., Beyersdorf, A. J., Thornhill, K. L., et al. (2012). Spectral absorption of biomass burning aerosol determined from retrieved single scattering albedo during ARCTAS. *Atmospheric Chemistry and Physics*, *12*(21), 10,505–10,518. https://doi.org/10.5194/acp-12-10505-2012

Costantino, L., & Breon, F. M. (2010). Analysis of aerosol-cloud interaction from multi-sensor satellite observations. *Geophysical Research Letters*, *37*, L11801. https://doi.org/10.1029/2009GL041828

Costantino, L., & Breon, F. M. (2013). Aerosol indirect effect on warm clouds over south-east Atlantic, from co-located MODIS and CALIPSO observations. *Atmospheric Chemistry and Physics*, *13*(1), 69–88. https://doi.org/10.5194/acp-13-69-2013

Dadashazar, H., Braun, R. A., Crosbie, E., Chuang, P. Y., Woods, R. K., Jonsson, H. H., & Sorooshian, A. (2018). Aerosol characteristics in the entrainment interface layer in relation to the marine boundary layer and free troposphere. *Atmospheric Chemistry and Physics*, *18*(3), 1495–1506. https://doi.org/10.5194/acp-18-1495-2018

Dadashazar, H., Wang, Z., Crosbie, E., Brunke, M., Zeng, X. B., Jonsson, H., et al. (2017). Relationships between giant sea salt particles and clouds inferred from aircraft physicochemical data. *Journal of Geophysical Research: Atmospheres*, *122*, 3421–3434. https://doi.org/10.1002/2016JD026019

Damoah, R., Spichtinger, N., Forster, C., James, P., Mattis, I., Wandinger, U., et al. (2004). Around the world in 17 days-hemispheric-scale transport of forest fire smoke from Russia in May 2003. *Atmospheric Chemistry and Physics*, *4*, 1311–1321. https://doi.org/10.5194/acp-4-1311-2004

de Gouw, J. A., Warneke, C., Parrish, D. D., Holloway, J. S., Trainer, M., & Fehsenfeld, F. C. (2003). Emission sources and ocean uptake of acetonitrile (CH3CN) in the atmosphere. *Journal of Geophysical Research*, *108*(D11), 4329. https://doi.org/10.1029/2002JD002897

Dennison, P. E., Brewer, S. C., Arnold, J. D., & Moritz, M. A. (2014). Large wildfire trends in the western United States, 1984–2011. *Geophysical Research Letters*, *41*, 2928–2933. https://doi.org/10.1002/2014GL059576

Devasthale, A., & Thomas, M. A. (2011). A global survey of aerosol-liquid water cloud overlap based on four years of CALIPSO-CALIOP data. *Atmospheric Chemistry and Physics*, *11*(3), 1143–1154. https://doi.org/10.5194/acp-11-1143-2011

Duong, H. T., Sorooshian, A., Craven, J. S., Hersey, S. P., Metcalf, A. R., Zhang, X. L., et al. (2011). Water-soluble organic aerosol in the Los Angeles basin and outflow regions: Airborne and ground measurements during the 2010 CALNEX field campaign. *Journal of Geophysical Research*, *116*, D00V04. https://doi.org/10.1029/2011JD016674

Flannigan, M. D., Stocks, B. J., & Wotton, B. M. (2000). Climate change and forest fires. *Science of the Total Environment*, *262*(3), 221–229. https://doi.org/10.1016/S0048-9697(00)00524-6

Formenti, P., Elbert, W., Maenhaut, W., Haywood, J., Osborne, S., & Andreae, M. O. (2003). Inorganic and carbonaceous aerosols during the Southern African Regional Science Initiative (SAFARI 2000) experiment: Chemical characteristics, physical properties, and emission data for smoke from African biomass burning. *Journal of Geophysical Research*, *108*(D13), 8488. https://doi.org/10.1029/2002JD002408

Fu, Q., & Liou, K. N. (1992). On the correlated k-distribution method for radiative-transfer in nonhomogeneous atmospheres. *Journal of the Atmospheric Sciences*, *49*(22), 2139–2156. https://doi.org/10.1175/1520-0469

Gao, S., Hegg, D. A., Hobbs, P. V., Kirchstetter, T. W., Magi, B. I., & Sadilek, M. (2003). Water-soluble organic components in aerosols associated with savanna fires in southern Africa: Identification, evolution, and distribution. *Journal of Geophysical Research*, *108*(D13), 8491. https://doi.org/10.1029/2002JD002324

Ge, C., Wang, J., Reid, J. S., Posselt, D. J., Xian, P., & Hyer, E. (2017). Mesoscale modeling of smoke transport from equatorial Southeast Asian maritime continent to the Philippines: First comparison of ensemble analysis with in situ observations. *Journal of Geophysical Research: Atmospheres*, *122*, 5380–5398. https://doi.org/10.1002/2016JD026241

Gerber, H., Arends, B. G., & Ackerman, A. S. (1994). New microphysics sensor for aircraft use. *Atmospheric Research*, *31*(4), 235–252. https://doi.org/10.1016/0169-8095(94)90001-9

Grieshop, A. P., Logue, J. M., Donahue, N. M., & Robinson, A. L. (2009). Laboratory investigation of photochemical oxidation of organic aerosol from wood fires 1: Measurement and simulation of organic aerosol evolution. *Atmospheric Chemistry and Physics*, *9*(4), 1263–1277. https://doi.org/10.5194/acp-9-1263-2009

Hair, J. W., Hostetler, C. A., Cook, A. L., Harper, D. B., Ferrare, R. A., Mack, T. L., et al. (2008). Airborne high spectral resolution lidar for profiling aerosol optical properties. *Applied Optics*, *47*(36), 6734–6752. https://doi.org/10.1364/Ao.47.006734

Hawkins, L. N., & Russell, L. M. (2010). Oxidation of ketone groups in transported biomass burning aerosol from the 2008 northern California lightning series fires. *Atmospheric Environment*, *44*(34), 4142–4154. https://doi.org/10.1016/j.atmosenv.2010.07.036

Haywood, J. M., Osborne, S. R., Francis, P. N., Keil, A., Formenti, P., Andreae, M. O., & Kaye, P. H. (2003). The mean physical and optical properties of regional haze dominated by biomass burning aerosol measured from the C-130 aircraft during SAFARI 2000. *Journal of Geophysical Research*, *108*(D13). https://doi.org/10.1029/2002JD002226

Heald, C. L., Coe, H., Jimenez, J. L., Weber, R. J., Bahreini, R., Middlebrook, A. M., et al. (2011). Exploring the vertical profile of atmospheric organic aerosol: Comparing 17 aircraft field campaigns with a global model. *Atmospheric Chemistry and Physics*, *11*(24), 12673–12696. https://doi.org/10.5194/acp-11-12673-2011

Hogan, T. F., Liu, M., Ridout, J. S., Peng, M. S., Whitcomb, T. R., Ruston, B. C., et al. (2014). The navy global environmental model. *Oceanography, Special Issue on Navy Operational Models*, *27*(3), 116–125.

Hu, Y. X., & Stamnes, K. (1993). An accurate parameterization of the radiative properties of water clouds suitable for use in climate models. *Journal of Climate*, *6*(4), 728–742. https://doi.org/10.1175/1520-0442(1993)006<0728:Aapotr>2.0.Co;2

Hyer, E. J., Reid, J. S., & Zhang, J. (2011). An over-land aerosol optical depth data set for data assimilation by filtering, correction, and aggregation of MODIS collection 5 optical depth retrievals. *Atmospheric Measurement Techniques*, *4*(3), 379–408. https://doi.org/10.5194/amt-4-379-2011

Johnson, B. T., Osborne, S. R., Haywood, J. M., & Harrison, M. A. J. (2008). Aircraft measurements of biomass burning aerosol over West Africa during DABEX. *Journal of Geophysical Research*, *113*, D00C06. https://doi.org/10.1029/2007JD009451

Johnson, B. T., Shine, K. P., & Forster, P. M. (2004). The semi-direct aerosol effect: Impact of absorbing aerosols on marine stratocumulus. *Quarterly Journal of the Royal Meteorological Society*, *130*(599), 1407–1422. https://doi.org/10.1256/qj.03.61

Jung, E., Albrecht, B. A., Jonsson, H. H., Chen, Y. C., Seinfeld, J. H., Sorooshian, A., et al. (2015). Precipitation effects of giant cloud condensation nuclei artificially introduced into stratocumulus clouds. *Atmospheric Chemistry and Physics*, *15*(10), 5645–5658. https://doi.org/10.5194/acp-15-5645-2015

Kahn, R. A., Chen, Y., Nelson, D. L., Leung, F. Y., Li, Q. B., Diner, D. J., & Logan, J. A. (2008). Wildfire smoke injection heights: Two perspectives from space. *Geophysical Research Letters*, *35*, L04809. https://doi.org/10.1029/2007GL032165

Kahn, R. A., Li, W. H., Moroney, C., Diner, D. J., Martonchik, J. V., & Fishbein, E. (2007). Aerosol source plume physical characteristics from space-based multiangle imaging. *Journal of Geophysical Research*, *112*(D11). https://doi.org/10.1029/2006JD007647

Kaufman, Y. J., Koren, I., Remer, L. A., Rosenfeld, D., & Rudich, Y. (2005). The effect of smoke, dust, and pollution aerosol on shallow cloud development over the Atlantic Ocean. *Proceedings of the National Academy of Sciences of the United States of America*, *102*(32), 11207–11212. https://doi.org/10.1073/pnas.0505191102

Keil, A., & Haywood, J. M. (2003). Solar radiative forcing by biomass burning aerosol particles during SAFARI 2000: A case study based on measured aerosol and cloud properties. *Journal of Geophysical Research*, *108*(D13), 8467. https://doi.org/10.1029/2002jhd002315

Koch, D., & Del Genio, A. D. (2010). Black carbon semi-direct effects on cloud cover: Review and synthesis. *Atmospheric Chemistry and Physics*, *10*(16), 7685–7696. https://doi.org/10.5194/acp-10-7685-2010

Kondo, Y., Matsui, H., Moteki, N., Sahu, L., Takegawa, N., Kajino, M., et al. (2011). Emissions of black carbon, organic, and inorganic aerosols from biomass burning in North America and Asia in 2008. *Journal of Geophysical Research*, *116*, D08204. https://doi.org/10.1029/2010JD015152

Labonne, M., Breon, F. M., & Chevallier, F. (2007). Injection height of biomass burning aerosols as seen from a spaceborne lidar. *Geophysical Research Letters*, *34*, L11806. https://doi.org/10.1029/2007GL029311

Liu, Z. Y., Vaughan, M., Winker, D., Kittaka, C., Getzewich, B., Kuehn, R., et al. (2009). The CALIPSO lidar cloud and aerosol discrimination: Version 2 algorithm and initial assessment of performance. *Journal of Atmospheric and Oceanic Technology*, *26*(7), 1198–1213. https://doi.org/10.1175/2009jtecha1229.1

Lynch, P., Reid, J. S., Westphal, D. L., Zhang, J. L., Hogan, T. F., Hyer, E. J., et al. (2016). An 11-year global gridded aerosol optical thickness reanalysis (v1.0) for atmospheric and climate sciences. *Geoscientific Model Development*, *9*(4), 1489–1522. https://doi.org/10.5194/gmd-9-1489-2016

Markowicz, K. M., Lisok, J., & Xian, P. (2017). Simulations of the effect of intensive biomass burning in July 2015 on Arctic radiative budget. *Atmospheric Environment*, *171*, 248–260. https://doi.org/10.1016/j.atmosenv.2017.10.015

Martin, M. V., Logan, J. A., Kahn, R. A., Leung, F. Y., Nelson, D. L., & Diner, D. J. (2010). Smoke injection heights from fires in North America: Analysis of 5 years of satellite observations. *Atmospheric Chemistry and Physics*, *10*(4), 1491–1510. https://doi.org/10.5194/acp-10-1491-2010

Maudlin, L. C., Wang, Z., Jonsson, H. H., & Sorooshian, A. (2015). Impact of wildfires on size-resolved aerosol composition at a coastal California site. *Atmospheric Environment*, *119*, 59–68. https://doi.org/10.1016/j.atmosenv.2015.08.039

McClatchey, R., Fenn, R. W., Selby, J. E. A., Volz, F. E., & Garing, J. S. (1972). Optical properties of the atmosphere. Environmental Research Paper 411, Air Force Cambridge Research Laboratory, Environmental Research Paper 411, *Air Force Cambridge Research Laboratory*.

McMillan, W. W., Warner, J. X., Comer, M. M., Maddy, E., Chu, A., Sparling, L., et al. (2008). Airs views transport from 12 to 22 July 2004 Alaskan/Canadian fires: Correlation of AIRS CO and MODIS AOD with forward trajectories and comparison of airs co retrievals with DC-8 in situ measurements during INTEX-A/ICARTT. *Journal of Geophysical Research*, *113*, D20301. https://doi.org/10.1029/2007JD009711

Moritz, M. A., Parisien, M. A., Batllori, E., Krawchuk, M. A., Van Dorn, J., Ganz, D. J., & Hayhoe, K. (2012). Climate change and disruptions to global fire activity. *Ecosphere*, *3*(6), art49. https://doi.org/10.1890/Es11-00345.1

Muhle, J., Lueker, T. J., Su, Y., Miller, B. R., Prather, K. A., & Weiss, R. F. (2007). Trace gas and particulate emissions from the 2003 southern California wildfires. *Journal of Geophysical Research*, *112*, D03307. https://doi.org/10.1029/2006JD007350

Painemal, D., Kato, S., & Minnis, P. (2014). Boundary layer regulation in the Southeast Atlantic cloud microphysics during the biomass burning season as seen by the a-train satellite constellation. *Journal of Geophysical Research: Atmospheres*, *119*, 11,288–11,302. https://doi.org/10.1002/2014JD022182

Paugam, R., Wooster, M., Freitas, S., & Martin, M. V. (2016). A review of approaches to estimate wildfire plume injection height within large-scale atmospheric chemical transport models. *Atmospheric Chemistry and Physics*, *16*(2), 907–925. https://doi.org/10.5194/acp-16-907-2016

Pósfai, M., Simonics, R., Li, J., Hobbs, P. V., & Buseck, P. R. (2003). Individual aerosol particles from biomass burning in southern Africa: 1. Compositions and size distributions of carbonaceous particles. *Journal of Geophysical Research*, *108*(D13), 8483. https://doi.org/10.1029/2002JD002291

Prabhakar, G., Ervens, B., Wang, Z., Maudlin, L. C., Coggon, M. M., Jonsson, H. H., et al. (2014). Sources of nitrate in stratocumulus cloud water: Airborne measurements during the 2011 E-PEACE and 2013 NiCE studies. *Atmospheric Environment*, *97*, 166–173. https://doi.org/10.1016/j.atmosenv.2014.08.019

Rajapakshe, C., Zhang, Z. B., Yorks, J. E., Yu, H. B., Tan, Q., Meyer, K., et al. (2017). Seasonally transported aerosol layers over Southeast Atlantic are closer to underlying clouds than previously reported. *Geophysical Research Letters*, *44*, 5818–5825. https://doi.org/10.1002/2017GL073559

Reid, J. S., Hobbs, P. V., Ferek, R. J., Blake, D. R., Martins, J. V., Dunlap, M. R., & Liousse, C. (1998). Physical, chemical, and optical properties of regional hazes dominated by smoke in Brazil. *Journal of Geophysical Research*, *103*(D24), 32,059–32,080. https://doi.org/10.1029/98JD00458

Reid, J. S., Hyer, E. J., Prins, E. M., Westphal, D. L., Zhang, J. L., Wang, J., et al. (2009). Global monitoring and forecasting of biomass-burning smoke: Description of and lessons from the fire locating and modeling of burning emissions (FLAMBE) program. *Ieee Journal of Selected Topics in Applied Earth Observations and Remote Sensing*, *2*(3), 144–162. https://doi.org/10.1109/Jstars.2009.2027443

Reid, J. S., Koppmann, R., Eck, T. F., & Eleuterio, D. P. (2005). A review of biomass burning emissions part II: Intensive physical properties of biomass burning particles. *Atmospheric Chemistry and Physics*, *5*, 799–825. https://doi.org/10.5194/acp-5-799-2005

Reid, J. S., Lagrosas, N. D., Jonsson, H. H., Reid, E. A., Atwood, S. A., Boyd, T. J., et al. (2016). Aerosol meteorology of maritime continent for the 2012 7SEAS southwest monsoon intensive study—Part 2: Philippine receptor observations of fine-scale aerosol behavior. *Atmospheric Chemistry and Physics*, *16*(22), 14057–14078. https://doi.org/10.5194/acp-16-14057-2016

Reid, J. S., Lagrosas, N. D., Jonsson, H. H., Reid, E. A., Sessions, W. R., Simpas, J. B., et al. (2015). Observations of the temporal variability in aerosol properties and their relationships to meteorology in the summer monsoonal South China Sea/East Sea: The scale-dependent role of monsoonal flows, the Madden-Julian Oscillation, tropical cyclones, squall lines and cold pools. *Atmospheric Chemistry and Physics*, *15*(4), 1745–1768. https://doi.org/10.5194/acp-15-1745-2015

Reid, J. S., Xian, P., Hyer, E. J., Flatau, M. K., Ramirez, E. M., Turk, F. J., et al. (2012). Multi-scale meteorological conceptual analysis of observed active fire hotspot activity and smoke optical depth in the maritime continent. *Atmospheric Chemistry and Physics*, *12*(4), 2117–2147. https://doi.org/10.5194/acp-12-2117-2012

Rose, F. G., Rutan, D. A., Charlock, T., Smith, G. L., & Kato, S. (2013). Algorithm for the constraining of radiative transfer calculations to CERES-observed broadband top-of-atmosphere irradiance. *Journal of Atmospheric and Oceanic Technology*, *30*(6), 1091–1106. https://doi.org/10.1175/Jtech-D-12-00058.1

Sahu, L. K., Kondo, Y., Moteki, N., Takegawa, N., Zhao, Y., Cubison, M. J., et al. (2012). Emission characteristics of black carbon in anthropogenic and biomass burning plumes over California during ARCTAS-CARB 2008. *Journal of Geophysical Research*, *117*, D16302. https://doi.org/10.1029/2011JD017401

Schlosser, J. S., Braun, R. A., Bradley, T., Dadashazar, H., MacDonald, A. B., Aldhaif, A. A., et al. (2017). Analysis of aerosol composition data for western United States wildfires between 2005 and 2015: Dust emissions, chloride depletion, and most enhanced aerosol constituents. *Journal of Geophysical Research: Atmospheres*, *122*, 8951–8966. https://doi.org/10.1002/2017JD026547

Shingler, T., Crosbie, E., Ortega, A., Shiraiwa, M., Zuend, A., Beyersdorf, A., et al. (2016). Airborne characterization of subsaturated aerosol hygroscopicity and dry refractive index from the surface to 6.5 km during the SEAC^{4}RS campaign. *Journal of Geophysical Research: Atmospheres*, *121*, 4188–4210. https://doi.org/10.1002/2015JD024498

Simoneit, B. R. T. (2002). Biomass burning—A review of organic tracers for smoke from incomplete combustion. *Applied Geochemistry*, *17*(3), 129–162. https://doi.org/10.1016/S0883-2927(01)00061-0

Singh, H. B., Anderson, B. E., Brune, W. H., Cai, C., Cohen, R. C., Crawford, J. H., et al. (2010). Pollution influences on atmospheric composition and chemistry at high northern latitudes: Boreal and California forest fire emissions. *Atmospheric Environment*, *44*(36), 4553–4564. https://doi.org/10.1016/j.atmosenv.2010.08.026

Singh, H. B., Salas, L., Herlth, D., Kolyer, R., Czech, E., Viezee, W., et al. (2003). In situ measurements of HCN and CH3CN over the Pacific Ocean: Sources, sinks, and budgets. *Journal of Geophysical Research*, *108*(D20), 8795. https://doi.org/10.1029/2002JD003006

Sofiev, M., Vankevich, R., Ermakova, T., & Hakkarainen, J. (2013). Global mapping of maximum emission heights and resulting vertical profiles of wildfire emissions. *Atmospheric Chemistry and Physics*, *13*(14), 7039–7052. https://doi.org/10.5194/acp-13-7039-2013

Sorooshian, A., Brechtel, F. J., Ma, Y. L., Weber, R. J., Corless, A., Flagan, R. C., & Seinfeld, J. H. (2006). Modeling and characterization of a particle-into-liquid sampler (PILS). *Aerosol Science and Technology*, *40*(6), 396–409. https://doi.org/10.1080/02786820600632282

Sorooshian, A., Crosbie, E., Maudlin, L. C., Youn, J. S., Wang, Z., Shingler, T., et al. (2015). Surface and airborne measurements of organosulfur and methanesulfonate over the western United States and coastal areas. *Journal of Geophysical Research: Atmospheres*, *120*, 8535–8548. https://doi.org/10.1002/2015JD023822

Sorooshian, A., MacDonald, A. B., Dadashazar, H., Bates, K. H., Coggon, M. M., Craven, J. S., et al. (2017). A multi-year data set on aerosol-cloud-precipitation-meteorology interactions for marine stratocumulus clouds. *Figshare*. https://doi.org/10.6084/m9.figshare.5099983.v3

Sorooshian, A., MacDonald, A. B., Dadashazar, H., Bates, K. H., Coggon, M. M., Craven, J. S., et al. (2018). A multi-year data set on aerosol-cloud-precipitation-meteorology interactions for marine stratocumulus clouds. *Scientific Data*, *5*, 180026. https://doi.org/10.1038/sdata.2018.26

Trentmann, J., Andreae, M. O., Graf, H. F., Hobbs, P. V., Ottmar, R. D., & Trautmann, T. (2002). Simulation of a biomass-burning plume: Comparison of model results with observations. *Journal of Geophysical Research*, *107*(D2), 4013. https://doi.org/10.1029/2001JD000410

Turton, J. D., & Nicholls, S. (1987). A study of the diurnal-variation of stratocumulus using a multiple mixed layer model. *Quarterly Journal of the Royal Meteorological Society*, *113*(477), 969–1009. https://doi.org/10.1256/smsqj.47710

Walter, C., Freitas, S. R., Kottmeier, C., Kraut, I., Rieger, D., Vogel, H., & Vogel, B. (2016). The importance of plume rise on the concentrations and atmospheric impacts of biomass burning aerosol. *Atmospheric Chemistry and Physics*, *16*(14), 9201–9219. https://doi.org/10.5194/acp-16-9201-2016

Wang, J., Ge, C., Yang, Z. F., Hyer, E. J., Reid, J. S., Chew, B. N., et al. (2013). Mesoscale modeling of smoke transport over the Southeast Asian maritime continent: Interplay of sea breeze, trade wind, typhoon, and topography. *Atmospheric Research*, *122*, 486–503. https://doi.org/10.1016/j.atmosres.2012.05.009

Wang, Z., Ramirez, M. M., Dadashazar, H., MacDonald, A. B., Crosbie, E., Bates, K. H., et al. (2016). Contrasting cloud composition between coupled and decoupled marine boundary layer clouds. *Journal of Geophysical Research: Atmospheres*, *121*, 11,679–11,691. https://doi.org/10.1002/2016JD025695

Wang, Z., Sorooshian, A., Prabhakar, G., Coggon, M. M., & Jonsson, H. H. (2014). Impact of emissions from shipping, land, and the ocean on stratocumulus cloud water elemental composition during the 2011 E-PEACE field campaign. *Atmospheric Environment*, *89*, 570–580. https://doi.org/10.1016/j.atmosenv.2014.01.020

Wonaschutz, A., Hersey, S. P., Sorooshian, A., Craven, J. S., Metcalf, A. R., Flagan, R. C., & Seinfeld, J. H. (2011). Impact of a large wildfire on water-soluble organic aerosol in a major urban area: The 2009 Station Fire in Los Angeles county. *Atmospheric Chemistry and Physics*, *11*(16), 8257–8270. https://doi.org/10.5194/acp-11-8257-2011

Xian, P., Reid, J. S., Atwood, S. A., Johnson, R. S., Hyer, E. J., Westphal, D. L., & Sessions, W. (2013). Smoke aerosol transport patterns over the maritime continent. *Atmospheric Research*, *122*, 469–485. https://doi.org/10.1016/j.atmosres.2012.05.006

Yamaguchi, T., Feingold, G., Kazil, J., & McComiskey, A. (2015). Stratocumulus to cumulus transition in the presence of elevated smoke layers. *Geophysical Research Letters*, *42*, 10,478–10,485. https://doi.org/10.1002/2015GL066544

Yokelson, R. J., Crounse, J. D., DeCarlo, P. F., Karl, T., Urbanski, S., Atlas, E., et al. (2009). Emissions from biomass burning in the Yucatan. *Atmospheric Chemistry and Physics*, *9*(15), 5785–5812. https://doi.org/10.5194/acp-9-5785-2009

Yu, H. B., Zhang, Y., Chin, M., Liu, Z. Y., Omar, A., Remer, L. A., et al. (2012). An integrated analysis of aerosol above clouds from A-Train multi-sensor measurements. *Remote Sensing of Environment*, *121*, 125–131. https://doi.org/10.1016/j.rse.2012.01.011

Zhang, J. L., & Reid, J. S. (2006). MODIS aerosol product analysis for data assimilation: Assessment of over-ocean level 2 aerosol optical thickness retrievals. *Journal of Geophysical Research*, *111*, D22207. https://doi.org/10.1029/2005JD006898